Search for Supersymmetric Particles in $\bar{p}p$ Collisions at $\sqrt{s} = 1.8$ TeV

by Ping Hu

A dissertation submitted to the

Graduate School— New Brunswick

Rutgers, The State University of New Jersey

in partial fulfillment of the requirements

for the degree of

Doctor of Philosophy

Graduate Program in Physics

Written under the direction of

Professor Thomas J. Devlin

and approved by

T. J. Devlin

Y. Kojima

C. Loselaco

F. Sannes

New Brunswick, New Jersey

October, 1990

HAB1826

FERMILAB
LIBRARY

ABSTRACT OF THE DISSERTATION

Search for Supersymmetric Particles in $\bar{p}p$ Collisions at $\sqrt{s} = 1.8$ TeV

by Ping Hu . Ph.D.

Dissertation Director: Professor Thomas J. Devlin

Supersymmetry is a proposed symmetry that links fermions and bosons. In this theory all fundamental fermions and bosons have supersymmetic partners with properties differing only by spin (and mass). If supersymmetry is connected with the origin of the electroweak scale, then supersymmetric particles may exist with masses accessible at the Tevatron collider. In the minimal supersymmetry model, the squarks and gluino can be produced in $\bar{p}p$ collision. Assume the photino is the lightest supersymmetric particle, it could escape the detector. If the other gauge particles' masses are higher than squarks and gluino's, the dominant decay mode of squarks and gluino is to the normal quarks with photino. A study of data set collected in 1988-89 run by CDF collaboration is discussed in this thesis. The results show that the data is in good agreement with the Standard Model prediction, and the lower mass limits for squark and gluino were set based on the study.

Acknowledgements

I would like to thank my advisor. T. Devlin. who provided me the opportunity to work at CDF experiment and suggested this thesis topic. Without his support this thesis would be impossible.

I also thank all my colleagues at CDF, whose names are listed at the end of the thesis, for their efforts to make this experiment run successfully. In particular, I thank Jim Freeman for his advice about this thesis. and his experience on this topic has been much helpful for my data analysis. And I owe my thanks to many people in the collaboration for their willingness to discuss with me, and those discussions were very beneficial for my study.

I have my special thanks to Dr. T. D. Lee of Columbia University, who sponsored the CUSPEA program which gave me the opportunity to come to the United State to pursue my PhD degree. And I also thank Dr. G. Trilling of University of California at Berkeley, who encouraged me to work on high energy experimental physics when he interviewed me in China.

Finally, I thank my wife, Jia Wang, for her constant support and encouragement.

Table of Contents

Abstract ii

Acknowledgements iii

List of Tables iv

List of Figures v

1. Introduction 1

2. Theory and Previous Experiments 4

2.1. Supersymmetry Theory 4

2.1.1. SUSY Particle Spectrum and R Parity 5

2.2. SUSY Mass Spectrum 6

2.2.1. Gauginos 6

2.2.2. Squarks and Sleptons 7

2.3. The Minimal SUSY Model 8

2.4. Production of Squark and Gluino in $\bar{p}p$ collision 13

2.5. Previous Experimental SUSY Searches 14

3. Experiment Apparatus and Particle Detection 17

3.1. Tevatron 17

3.2. Collider Detector at Fermilab 19

3.2.1. Trigger Counters and Luminosity Monitoring 20

3.2.2. Vertex Time Projection Chamber 20

3.2.3. Central Tracking Chamber 20

3.2.4. Superconducting Solenoid Magnet Coil 23
3.2.5. Calorimeters 23
3.2.6. Central Muon Chamber 25
3.2.7. Level 0, Level 1 and Level 2 Trigger System 26
3.2.8. Data Acquisition System 27
3.2.9. Level 3 28
3.3. Trigger and Data Collection 30
3.3.1. Trigger 30
3.3.2. Data Collection 31

4. Data Analysis: Event Selection 33
4.1. Spin Cycle and Production 34
4.1.1. Spin Cycle 34
4.1.2. Spin Production 34
4.2. Further Selection on $\not{E}_T$ Events 37
4.3. SUSY Selection 37

5. Data Analysis: Background Study 43
5.1. $W \rightarrow e + \nu$ 45
5.2. $W \rightarrow \mu + \nu$ 47
5.3. $W \rightarrow \tau + \nu$ 52
5.4. $Z \rightarrow \nu\bar{\nu}$ 54
5.5. QCD Events 59
5.6. Summary 59

6. Data Analysis: Monte Carlo Study of SUSY Signal 64

7. Data Analysis: SUSY Particle Mass Limits 67
7.1. $M_{\tilde{q}} < M_{\tilde{g}}$ 67

List of Figures

2.1. $\tilde{\gamma}$-quark, $\tilde{\gamma}$-electron interactions 9

2.2. $\tilde{q}, \tilde{g}$ production processes 10

2.3. $\tilde{q}, \tilde{g}$ production processes 11

2.4. $\tilde{q}, \tilde{g}$ decay to $\tilde{\gamma}$ 12

2.5. Total cross sections vs. SUSY particle masses 15

2.6. Squark and gluino mass limits from previous experiments. 16

3.1. Fermilab accelerator complex 18

3.2. Cross section view of CDF detector 21

3.3. CDF detector 22

3.4. Energy resolutions of central and endwall hadron calorimeters . . 24

3.5. Data flow in the CDF data acquisition system 29

4.1. $\Delta\phi$ between $\not{E}_T$ and the third jet 40

4.2. $\not{E}_T$ distribution of the selected data sample 41

4.3. Jet multiplicity of the selected data sample 42

5.1. W + jet and Z + jet processes from $\bar{p}p$ collision 44

5.2. Background from Stirling Monte Carlo $W \rightarrow e\nu_e$ processes 46

5.3. Background from $W \rightarrow e\nu_e$ process estimated from data 48

5.4. Background from Stirling Monte Carlo $W \rightarrow \mu\nu_\mu$ processes 49

5.5. Background from $W \rightarrow \mu\nu_\mu$ process estimated from data 51

5.6. Background from Stirling Monte Carlo $W \rightarrow \tau\nu_\tau$ processes 53

5.7. Background from $W \rightarrow \tau\nu_\tau$ process estimated from data 55

5.8. Background from Stirling Monte Carlo $Z \rightarrow \nu\bar{\nu}$ processes 56

5.9. $W(Z)$ P_T distribution in $W(Z)$ – jets events 57

5.10. Background from $Z \rightarrow \nu\bar{\nu}$ process estimated from data 58

5.11. $\Delta\phi$ between $\not{E}_T$ and the third jet 60

5.12. $\not{E}_T$ distribution for $W(Z)$ – jet(s) background from STIRLING . 61

5.13. $\not{E}_T$ distribution for background estimated from CDF data sample 63

6.1. $\not{E}_T$ distribution of SUSY processes 65

7.1. SUSY particle mass limits 70

7.2. $M_{\tilde{q}} > M_{\tilde{g}}$ 69

8. Summary 71

Appendix A. The Colliders 72

Appendix B. Cuts Used in Spin Cycle 74

Appendix C. $W \rightarrow e - \nu$ Selection 1 76

Appendix D. $W \rightarrow e - \nu$ Selection 2 78

Appendix E. Method Used in Determination of the Upper Limit 80

References 83

Vita 88

List of Tables

1.1. Three generations of fundamental spin-$\frac{1}{2}$ particles 2

1.2. Fundamental forces and gauge bosons 2

2.1. SUSY particle spectrum 5

3.1. CDF calorimeter performance 26

4.1. Data path and cuts 35

7.1. Expected SUSY events from Monte Carlo 68

7.2. Expected SUSY events from Monte Carlo 69

Chapter 1
Introduction

Elementary particle physics has undergone great advances in the last two decades. During this time. electromagnetic interactions and weak interactions were unified in the electroweak theory [1]-[3] described by Glashow, Weinberg and Salam. Quantum Chromodynamics (QCD) [4]-[6] has emerged as a comprehensive description of the strong interactions. Together, these theories are often called "The Standard Model".

Throughout these decades, experiments added pieces to the standard model. In 1974 J/ψ particle was discovered. This was the first experimental evidence of existence of charm quark which was required by the GIM mechanism [7]. Later in the 1970's the τ lepton and the bottom quark were also discovered. This extended the lepton and quark family to the third generation. Another crucial discovery in that decade was a neutral current component of the weak force.

In the 1980's, the focus of the experiments was on the colliders (see Appendix A). The trijet phenomenon was observed at an e^-e^- collider. This phenomenon is an important signature of gluon's existence and strong evidence supporting QCD. Then the last big piece of the electroweak puzzle left was the intermediate bosons W^+, W^- and Z^0. In 1983 such particles were discovered at CERN $Sp\bar{p}S$ collider with the masses predicted by theory.

At present the fundamental constituents of matter and the interactions among them have been simplified as following: all matter appears to be composed of quarks and leptons, which are pointlike, structureless, spin-$\frac{1}{2}$ particles (see Table 1.1). They interact each other by exchange of gauge bosons (see Table 1.2).

quark	charge	mass(GeV)	lepton	charge	mass(GeV)
up(u)	$\frac{2}{3}$	0.31	e-neutrino(ν_e)	0	$< 1.8 \times 10^{-8}$
down(d)	$-\frac{1}{3}$	0.31	electron(e)	-1	5.11×10^{-4}
charm(c)	$\frac{2}{3}$	1.5	μ-neutrino(ν_μ)	0	$< 2.5 \times 10^{-4}$
strange(s)	$-\frac{1}{3}$	0.5	muon(μ)	-1	0.106
top(t)	$\frac{2}{3}$	?	τ-neutrino(ν_τ)	0	$< 7 \times 10^{-2}$
bottom(b)	$-\frac{1}{3}$	4.5	tau(τ)	-1	1.78

Table 1.1: Three generations of fundamental spin-$\frac{1}{2}$ particles

force	gauge boson	charge	spin	mass
strong	gluon(g)	0	1	0
electromagnetic	photon(γ)	0	1	0
weak	W-boson($W^\pm$)	± 1	1	79.8
	Z-boson(Z^0)	0	1	91.1
gravitational	graviton(G)	0	2	0

Table 1.2: Fundamental forces and gauge bosons

There are four kinds of interactions: electromagnetic, weak, strong interactions and gravity. They are mediated by photon(γ), $W^\pm$, Z^0, gluon(g) and graviton. Quarks and leptons can be grouped into three generations (also called families) as shown in Table 1.1. The top quark has not been observed yet. The most recent top quark search at CDF collaboration has the result of lower limit of top quark mass of 89 GeV at 95% confidence level [8]. The τ-neutrino has been studied only as an un-detected final state particle in decays of $\tau^\pm$, which behave in a manner completely consistent with the Standard Model properties for the ν_τ. The recent experiments at SLAC (Stanford Linear Accelerator Collider) and LEP (Large Electron Position collider) have concluded that no fourth generation neutrino with

mass of less than 45 GeV exists [9 - 13]. The graviton has not been discovered. The quantum treatment of gravity is still an open question. In addition to the gauge bosons, a Higgs field is necessary for spontaneous symmetry breaking in the electro-weak theory. The Higgs particle *(H)* has not been discovered. The present lower limit of Higgs mass is 24 GeV [14].

The standard model works well in the energy scale accessible at present. But many theorists believe that it is incomplete. One outstanding question is: Could the strong interaction be unified with electroweak interaction? If the answer is yes, how to do it? The theories dealing with this question are called Grand Unification Theories (GUT). There are many models, all with the same signature — unification is reached at the energy scale of 10^{15} GeV. This raises another question called the *hierarchy problem* — how could the symmetry broken from such high energy generate the particles with very low masses at electroweak energy scale.

One of the solutions to the *hierarchy problem* is supersymmetry, a symmetry proposed between fermions and bosons. Fermions and bosons emerge as separate classes of particles when supersymmetry is broken, so that every particle would have a supersymmetric partner with the same properties except spin and mass. If supersymmetry is to contribute to the resolution of the *hierarchy problem*, the supersymmetric particles' masses should not be far above electroweak energy scale.

The objective of the study presented in this thesis is to search for evidence of supersymmetric particles in the energy region available at the Fermilab Collider. Chapter 2 reviews the theoretical background and previous experimental work. Chapter 3 describes briefly the experimental apparatus. Chapter 4 through Chapter 7 describe the data analysis and Chapter 8 summarizes the results.

Chapter 2

Theory and Previous Experiments

2.1 Supersymmetry Theory

Supersymmetry (SUSY) was invented in 1973 by Wess and Zumino [15], and has been discussed in many books [16]-[19]. It is a new kind of symmetry which relates fermions and bosons. In its simplest form, SUSY has a self-conjugate spin-$\frac{1}{2}$ Majorana generator Q_α which changes the total angular momentum by half a unit and turns a boson into a fermion and vice versa,

$$Q_\alpha|boson\rangle = |fermion\rangle,$$

$$Q_\alpha|fermion\rangle = |boson\rangle.$$

where $\alpha = 1, 2, 3, 4$ is a spinor index. Q_α satisfies the following commutation and anticommutation rules:

$$[Q_\alpha, M^{\mu\nu}] = i(\sigma^{\mu\nu}Q)_\alpha,$$

$$[Q_\alpha, P^\mu] = 0,$$

$$\{Q_\alpha, \bar{Q}_\beta\} = -2(\gamma_\mu)_{\alpha\beta}P^\mu,$$

$$\{Q_\alpha, Q_\beta\} = \{\bar{Q}_\alpha, \bar{Q}_\beta\}^+ = 0,$$

where γ^μ are the Dirac operators, $\sigma^{\mu\nu} = \frac{1}{4}[\gamma^\mu, \gamma^\nu]$, $\bar{Q}_\alpha = Q_\alpha^T\gamma^0$ and $M^{\mu\nu}, P^\mu$ are the generators of rotations and translations.

There could be N different operators $Q_\alpha^i (i = 1, \ldots, N)$ which satisfy the above requirement, but only SUSY with $N = 1$ allow fermions in chiral representations as observed.

Particle	Spin	Sparticle	Spin
lepton $l_{L,R}$	$\frac{1}{2}$	slepton $\tilde{l}_{L,R}$	0
quark $q_{L,R}$	$\frac{1}{2}$	squark $\tilde{q}_{L,R}$	0
photon γ	1	photino $\tilde{\gamma}$	$\frac{1}{2}$
gluon g	1	gluino $\tilde{g}$	$\frac{1}{2}$
$W^{\pm}$	1	wino $\tilde{W}^{\pm}$	$\frac{1}{2}$
Z^0	1	zino $\tilde{Z}^0$	$\frac{1}{2}$
Higgs $H_1^0, H_2^0, H^{\pm}$	0	shiggs $\tilde{H}_1^0, \tilde{H}_2^0, \tilde{H}^{\pm}$	$\frac{1}{2}$

Table 2.1: SUSY particle spectrum

2.1.1 SUSY Particle Spectrum and R Parity

Supersymmetry implies that each ordinary particle must have a corresponding supersymmetric partner. The SUSY particle spectrum is shown in Table 2.1. Since the observed particles lack boson-fermion degeneracy, supersymmetry must be broken.

In supersymmetry, particles are assigned to a quantum number usually called R-parity,

$$R = (-1)^{3B-L+2S}$$

where B is the baryon number, L is the lepton number and S is the spin. It is easy to see that R is $+1$ for usual particles and -1 for their SUSY partners. R parity is not necessarily conserved, but is imposed as a discrete symmetry.

In most SUSY models it is assumed that R parity is conserved. With this conservation, SUSY particles are always pair produced and decay to the lightest SUSY particle (LSP) which is stable.

2.2 SUSY Mass Spectrum

There are some stringent theoretical constraints on the SUSY mass spectrum. The gaugino masses are induced by gauge interactions involving loops of superheavy fields, giving

$$\frac{\mu_1}{\alpha_1} = \frac{\mu_2}{\alpha_2} = \frac{\mu_3}{\alpha_3}$$

at any mass scale. Here the μ_i are the gaugino masses of the U(1), SU(2) and SU(3) interactions and the $\alpha_i = g_i^2/4\pi$ are the couplings. So the gluino mass is

$$m_{\tilde{g}} = \mu_3 \, .$$

At the GUT scale there is a common gaugino mass μ and a common coupling g. For example, in SU(5) the above relation of μ_1 and μ_2 becomes

$$\frac{\mu_1}{\mu_2} = \frac{5}{3} \tan^2 \theta_W .$$

The photino and zino are defined as a linear combinations of gaugino fields $\tilde{W}_3$ and $\tilde{B}$ as following,

$$\tilde{\gamma} = \sin\theta_W \tilde{W}_3 + \cos\theta_W \tilde{B},$$

$$\tilde{Z} = \cos\theta_W \tilde{W}_3 - \sin\theta_W \tilde{B}.$$

2.2.1 Gauginos

At the W mass scale the SU(2) and U(1) gauginos mix with the Higgsinos and receive additional mass contributions from the Higgs vacuum expectation values v_1, v_2 and from a supersymmetric Higgsino mixing mass term m_1.

The mass terms $L = \frac{1}{2}\bar{\psi} M \psi$ of the Majorana fields in the neutralino sector are

$$\begin{pmatrix} \bar{\tilde{H}}_2^0, & \bar{\tilde{H}}_1^0, & \bar{\tilde{W}}_3, & \bar{\tilde{B}} \end{pmatrix} \frac{1}{2} \begin{pmatrix} 0 & -2m_1 & \frac{1}{\sqrt{2}} g v_2 & -\frac{1}{\sqrt{2}} g' v_2 \\ -2m_1 & 0 & -\frac{1}{\sqrt{2}} g v_1 & \frac{1}{\sqrt{2}} g' v_1 \\ \frac{1}{\sqrt{2}} g v_2 & -\frac{1}{\sqrt{2}} g v_1 & \mu_2 & 0 \\ -\frac{1}{\sqrt{2}} g' v_2 & \frac{1}{\sqrt{2}} g' v_1 & 0 & \mu_1 \end{pmatrix} \begin{pmatrix} \tilde{H}_2^0 \\ \tilde{H}_1^0 \\ \tilde{W}_3 \\ \tilde{B} \end{pmatrix}$$

where $(v_1^2 - v_2^2)^{1/2} = v = (\sqrt{2}G_F)^{-1/2}$. In general the neutralino mass eigenstates $\tilde{\chi}_1$, $\tilde{\chi}_2$, $\tilde{\chi}_3$ and $\tilde{\chi}_4$ are complex mixtures of the $\tilde{H}_1^0$, $\tilde{H}_2^0$, $\tilde{W}_3$ and $\tilde{B}$ states. It is not appropriate to think in terms of photino, zino and higgsino states.

In the chargino sector the mass matrix is

$$\begin{pmatrix} \tilde{W}, & \tilde{H}_{1L} - \tilde{H}_{2R} \end{pmatrix} \left[M \frac{1}{2}(1-\gamma_5) + M^T \frac{1}{2}(1-\gamma_5) \right] \begin{pmatrix} \tilde{W} \\ \tilde{H}_{1L} - \tilde{H}_{2R} \end{pmatrix}$$

where

$$M = \begin{pmatrix} \mu_2 & gv_1 \\ gv_2 & 2m_1 \end{pmatrix}.$$

2.2.2 Squarks and Sleptons

The squarks and sleptons have a common SUSY-breaking mass m_0 resulting from integrating out superheavy fields. And there are also mass contributions from diagrams with a gaugino and a fermion in the loop which are proportional to the gaugino masses. It can be expressed in terms of m_g. Finally there are scalar mass contributions from the supersymmetric "D-term" in the potential that are proportional to $v_2^2 - v_1^2$ in the minimal Higgs model. At the M_W scale the masses for the first generation are

$$m^2(\tilde{d}_L) = m_0^2 + 0.83m_{\tilde{g}}^2 + 0.43rM_Z^2,$$

$$m^2(\tilde{d}_R) = m_0^2 + 0.78m_{\tilde{g}}^2 - 0.07rM_Z^2,$$

$$m^2(\tilde{u}_L) = m_0^2 + 0.83m_{\tilde{g}}^2 - 0.36rM_Z^2,$$

$$m^2(\tilde{u}_R) = m_0^2 + 0.78m_{\tilde{g}}^2 - 0.14rM_Z^2,$$

$$m^2(\tilde{e}_L) = m_0^2 + 0.06m_{\tilde{g}}^2 + 0.28rM_Z^2,$$

$$m^2(\tilde{e}_R) = m_0^2 + 0.01m_{\tilde{g}}^2 + 0.22rM_Z^2,$$

$$m^2(\tilde{\nu}) = m_0^2 - 0.06m_{\tilde{g}}^2 - 0.50rM_Z^2,$$

where $r = (v_2^2 - v_1^2)/(v_1^2 + v_2^2)$.

2.3 The Minimal SUSY Model

In the previous section if we assume $\mu_1 = \mu_2 = 0$ and $v_1 = v_2$, then

$$m_{\tilde{\chi}_1} = 0.$$

$$m_{\tilde{\chi}_2} = \sqrt{m_1^2 - M_Z^2} - m_1.$$

$$m_{\tilde{\chi}_3} = 2m_1.$$

$$m_{\tilde{\chi}_4} = \sqrt{m_1^2 - M_Z^2} + m_1.$$

In this case $\tilde{\chi}_1$ is the photino and is massless. The squarks are nearly mass degenerate.

If the photino is the lightest supersymmetric particle (LSP), it interacts with matter through the processes in Figure 2.1. These processes' cross sections are very small. For example, the process $\tilde{\gamma}q$ has the cross section of the order

$$\sigma \simeq \frac{\alpha^2}{(m_{\tilde{q}})^4}\hat{s},$$

where $\hat{s}$ is the c.m.s energy square which is usually much smaller than $(m_{\tilde{q}})^2$. With the present limits of $m_{\tilde{e}} \geq 41$ GeV and $m_{\tilde{q}} \geq 70$ GeV, the photino interaction cross sections are less than 10 nb, on the order of neutrino cross section. The photino would escape the detector without generating any signal. Any such events would have large transverse momentum imbalance which is referred to as "missing E_T" ($\not{E}_T$).

In hadron-hadron collisions, the strongly interacting SUSY particles $\tilde{g}$ and $\tilde{q}$ can be pair produced via the QCD processes shown in Figure 2.2 and 2.3. We assume that the gaugino masses are high enough so that squarks and gluinos could only decay into photino and quarks as shown in Figure 2.4. The quarks would fragment into jets. In such case we could search for SUSY event signature by looking at the events with at least two jets and large $\not{E}_T$.

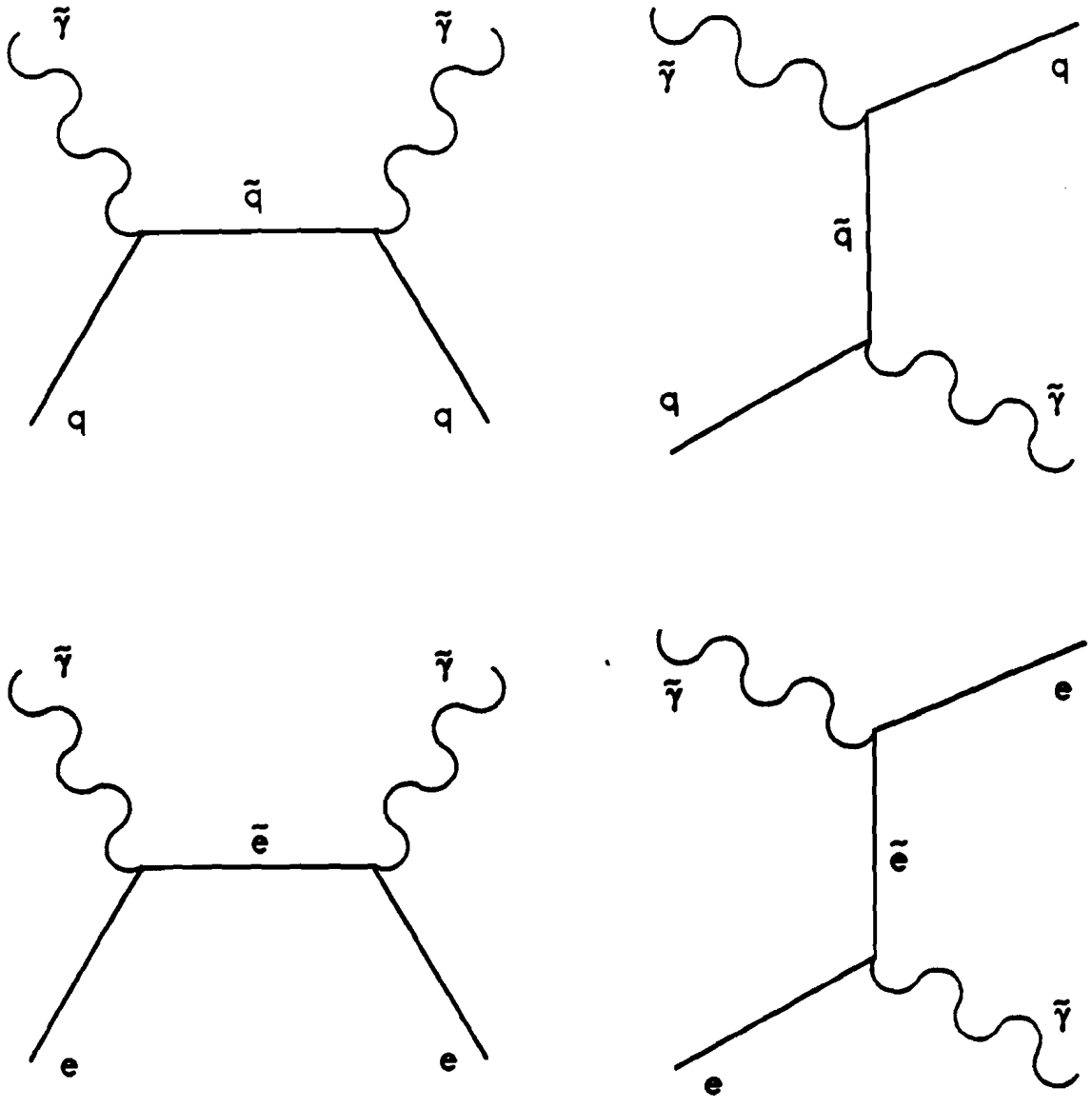

Figure 2.1: $\tilde{\gamma}$-quark, $\tilde{\gamma}$-electron interactions

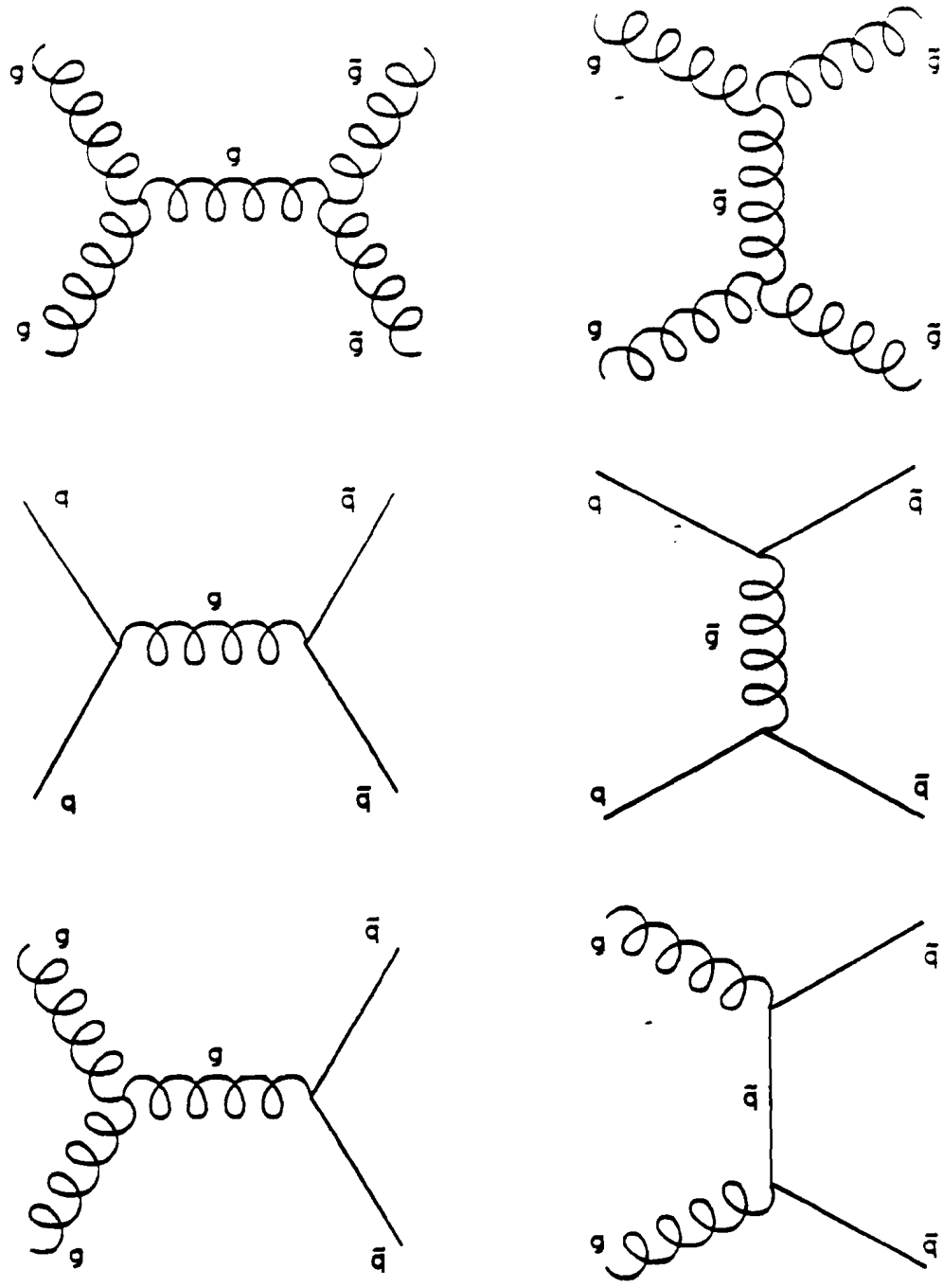

Figure 2.2: $\tilde{q}, \tilde{g}$ production processes

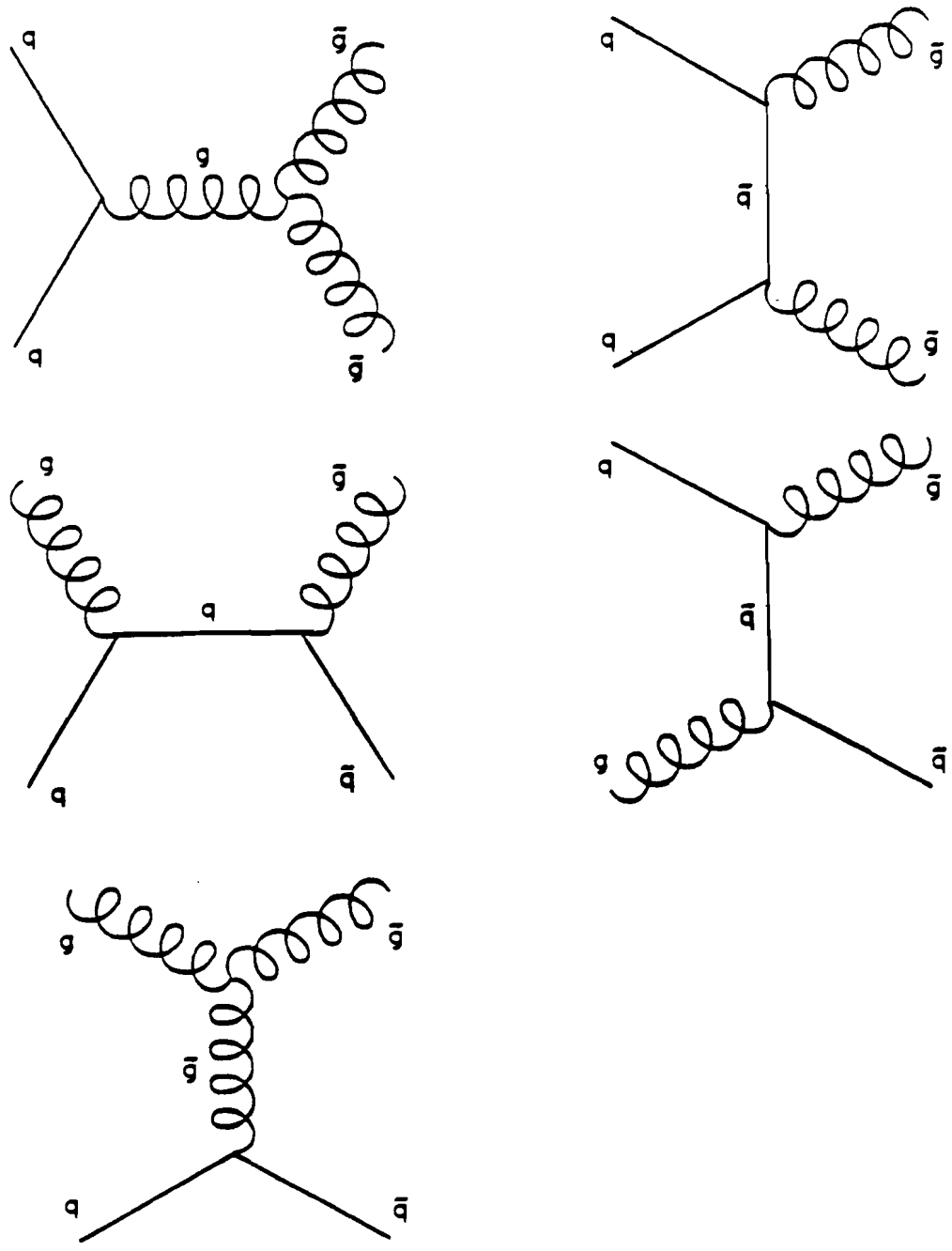

Figure 2.3: $\bar{q}, \bar{g}$ production processes

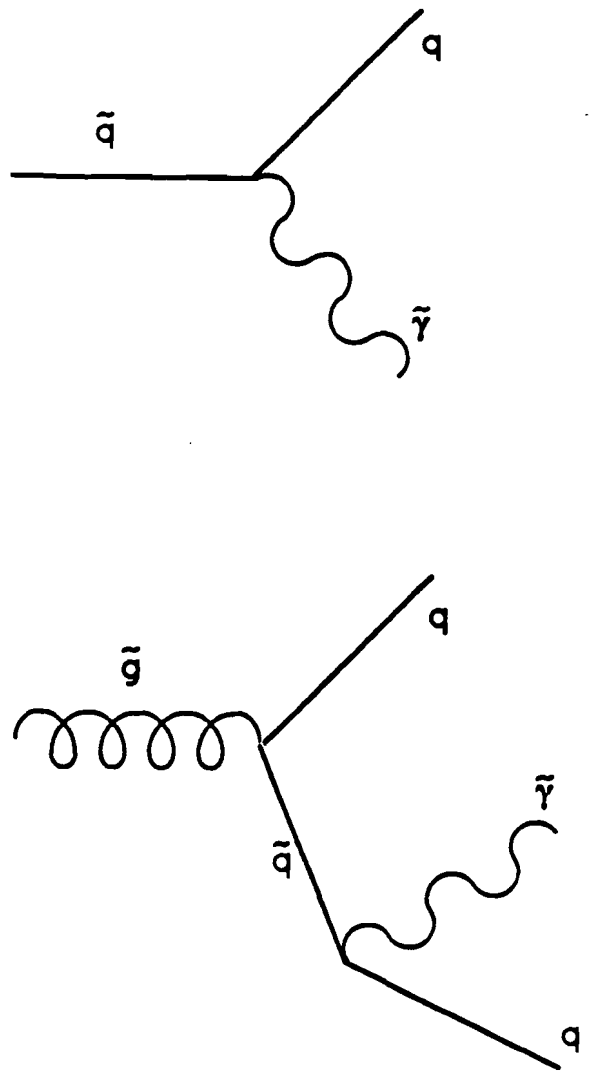

Figure 2.4: $\tilde{q}$ decays to q and $\tilde{\gamma}$ if $M_{\tilde{q}} < M_{\tilde{g}}$; $\tilde{g}$ decays to $q, \bar{q}$ and $\tilde{\gamma}$ via a virtual squark.

2.4 Production of Squark and Gluino in $\bar{p}p$ collision

The squark and gluino production cross sections from $\bar{p}p$ collision have been calculated in many papers [20]-[22]. From Figure 2.2 and 2.3 we can see that $\tilde{q}$ and $\tilde{g}$ are produced by the following processes: $gg \to \tilde{q}_i\bar{\tilde{q}}_i$, $q_iq_j \to \tilde{q}_i\tilde{q}_j$, $gq_i \to \tilde{g}\tilde{q}_i$, $gg \to \tilde{g}\tilde{g}$ and $q_i\bar{q}_i \to \tilde{g}\tilde{g}$. From parton model, the production cross sections of these processes are as following [20].

$$
\begin{aligned}
\sigma(gg \to \tilde{q}_i\bar{\tilde{q}}_i) &= \frac{\pi\alpha_s^2}{3\hat{s}^2}[(\frac{5}{8} + \frac{31}{4}\frac{m_{\tilde{q}}^2}{\hat{s}})\Phi + (4 + \frac{m_{\tilde{q}}^2}{\hat{s}})m_{\tilde{q}}^2 \ln(\frac{\hat{s}-\Phi}{\hat{s}+\Phi})], \\
\sigma(q_iq_j \to \tilde{q}_i\tilde{q}_j) &= \frac{4\pi\alpha_s^2}{9\hat{s}^2}[-2\Phi - (\hat{s} + \Delta_{\tilde{g}i} - \Delta_{\tilde{g}j})\Lambda_{\tilde{g}} + \frac{1}{1-\delta_{ij}}\frac{\Phi\hat{s}m_g^2}{\Delta_{\tilde{g}i}\Delta_{\tilde{g}j} - \hat{s}m_g^2} \\
&\quad -\frac{1}{3}\delta_{ij}\frac{\hat{s}m_{\tilde{g}^2}}{\hat{s} + \Delta_{\tilde{g}i} + \Delta_{\tilde{g}j}}\Lambda_{\tilde{g}}](1-\delta_{ij}), \\
\sigma(q_i\bar{q}_j \to \tilde{q}_i\bar{\tilde{q}}_j) &= \frac{4\pi\alpha_s^2}{27\hat{s}^2}\{3[-2\Phi - (\hat{s} + \Delta_{\tilde{g}i} - \Delta_{\tilde{g}j})\Lambda_{\tilde{g}} + \frac{\Phi\hat{s}m_g^2}{\Delta_{\tilde{g}i}\Delta_{\tilde{g}j} - \hat{s}m_g^2}] \\
&\quad +\delta_{ij}[\frac{\Phi^3}{\hat{s}^2} + \frac{\Phi(\hat{s} - \Delta_{\tilde{g}i} + \Delta_{\tilde{g}j})}{\hat{s}} + \frac{2(\Delta_{\tilde{g}i}\Delta_{\tilde{g}j} + \hat{s}m_g^2)}{\hat{s}}\Lambda_{\tilde{g}}]\}, \\
\sigma(gq_i \to \tilde{g}\tilde{q}_i) &= \frac{\pi}{\hat{s}^2}\{\frac{4\alpha_s^2}{9}\frac{\Phi}{2}(1 - \Delta/\hat{s}) + \alpha_s^2[2\Delta\Phi/\hat{s} + (\hat{s} + 2m_{\tilde{g}}^2)\bar{\Lambda}] \\
&\quad +\frac{4\alpha_s^2}{9}[\Phi(1 - 2\Lambda/\hat{s}) + (3m_{\tilde{q}}^2 - m_{\tilde{g}}^2)\Lambda] \\
&\quad -\alpha_s^2[\Phi(1 - \Delta/\hat{s}) + (m_{\tilde{q}}^2 - \Delta^2/\hat{s})\bar{\Lambda}] \\
&\quad +\frac{\alpha_s^2}{18}[\Phi(1 - 2\Delta/\hat{s}) + (m_{\tilde{g}}^2 + m_{\tilde{q}}^2 - 2\Delta^2/\hat{s})\Lambda] \\
&\quad +\frac{\alpha_s^2}{2}\{-[m_{\tilde{q}}^2 + m_{\tilde{g}}^2 + 2(m_{\tilde{q}}^4 - m_{\tilde{g}}^4)/\hat{s}]\Lambda \\
&\quad +[-2m_{\tilde{q}}^2 + 2(m_{\tilde{q}}^4 - m_{\tilde{g}}^4)/\hat{s}]\bar{\Lambda} - \Phi\}\}, \\
\sigma(gg \to \tilde{g}\tilde{g}) &= \frac{3\pi\alpha_s^2}{4\hat{s}}[3(1 + \frac{4m_{\tilde{g}}^2}{\hat{s}} - \frac{4m_{\tilde{g}}^4}{\hat{s}^2})\ln(\frac{\hat{s}+\Phi}{\hat{s}-\Phi}) - (4 + \frac{17m_{\tilde{g}}^2}{\hat{s}})\frac{\Phi}{\hat{s}}], \\
\sigma(q_i\bar{q}_i \to \tilde{g}\tilde{g}) &= \frac{\pi}{2\hat{s}^2}\{\frac{8\alpha_s^2}{3}\frac{\Phi}{3(\hat{s} - m_g^2)^2}(2\hat{s}^2 + 4m_{\tilde{g}}^2\hat{s}) + 2\{\frac{32\alpha_s^2}{27}[\Phi + 2\Delta_{\tilde{q}\tilde{g}}\Lambda_{\tilde{q}} \\
&\quad +\frac{\Phi\Delta_{\tilde{q}\tilde{g}}^2}{m_{\tilde{q}}^4 + m_{\tilde{g}}^4 + m_{\tilde{q}}^2(\hat{s} - 2m_{\tilde{g}}^2)}] + \frac{8\alpha_s^2}{3}\frac{1}{\hat{s} - m_g^2}[\Phi(m_{\tilde{q}}^2 - \frac{\hat{s} + 2m_{\tilde{g}}^2}{2}) \\
&\quad +(\Delta_{\tilde{q}\tilde{g}}^2 + m_{\tilde{g}}^2\hat{s})\Lambda_{\tilde{q}}]\} - \frac{8\alpha_s^2}{27}2\Lambda_{\tilde{q}}\frac{m_{\tilde{g}}^2\hat{s}}{\hat{s} - 2\Delta_{\tilde{q}\tilde{g}}}\}.
\end{aligned}
$$

In the above formulas, we used the following quantities

$$
\begin{aligned}
\Phi &= \hat{s} - (m_1 - m_2)^2 - 1/2 \hat{s} + (m_1 - m_2)^2 - 1/2, \\
\Delta_{ij} &= m_i^2 - m_j^2, \\
\Lambda_i &= \ln\left(\frac{\hat{s} - \Delta_{i1} - \Delta_{i2} - \Phi}{\hat{s} + \Delta_{i1} - \Delta_{i2} - \Phi}\right), \\
\Delta &= m_{\tilde{q}}^2 - m_{\tilde{g}}^2, \\
\Lambda &= \ln\left(\frac{\Delta + \hat{s} - \Phi}{\Delta + \hat{s} + \Phi}\right), \\
\tilde{\Lambda} &= \ln\left(\frac{\Delta - \hat{s} - \Phi}{\Delta - \hat{s} + \Phi}\right).
\end{aligned}
$$

Where m_1, m_2 are the masses of two final state particles and $\hat{s}$ is the square of c.m. energy of the two partons.

Assuming that all squarks are mass degenerate, the production cross sections for squark pair and gluino pair are shown in Figure 2.5.

2.5 Previous Experimental SUSY Searches

The SUSY particle searches have been performed in many experiments. At e^+e^- colliders, the most recent results are from TRISTAN [23]-[25] and LEP [26,27]. At $\bar{p}p$ colliders, the study has been done by UA1 [28]. The CDF collaboration did a study using a monojet data sample from 1987 run [29]. Most recently UA2 performed a SUSY search [30,31]. The highest limits reached in these experiments are $m_{\tilde{l}} > 41$ GeV [27], $m_{\tilde{\chi}} > 45$ GeV [27], $m_{\tilde{W}} > 45$ GeV [31], $m_{\tilde{q}} > 79$ GeV [30] and $m_{\tilde{g}} > 74$ GeV [30]. The current limits on squark and gluino masses are shown in Figure 2.6.

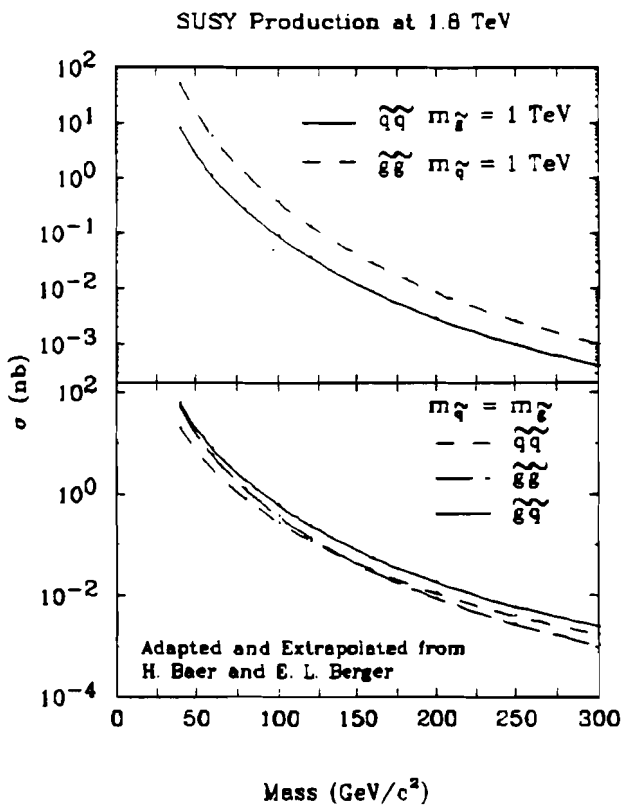

Figure 2.5: Total cross sections vs. SUSY particle masses at $\sqrt{s}$ = 1.8 TeV. It is derived from Baer and Berger's calculation in mass range 40-120 GeV/c^2 [21], and extrapolated as function $\sigma = aM^b$.

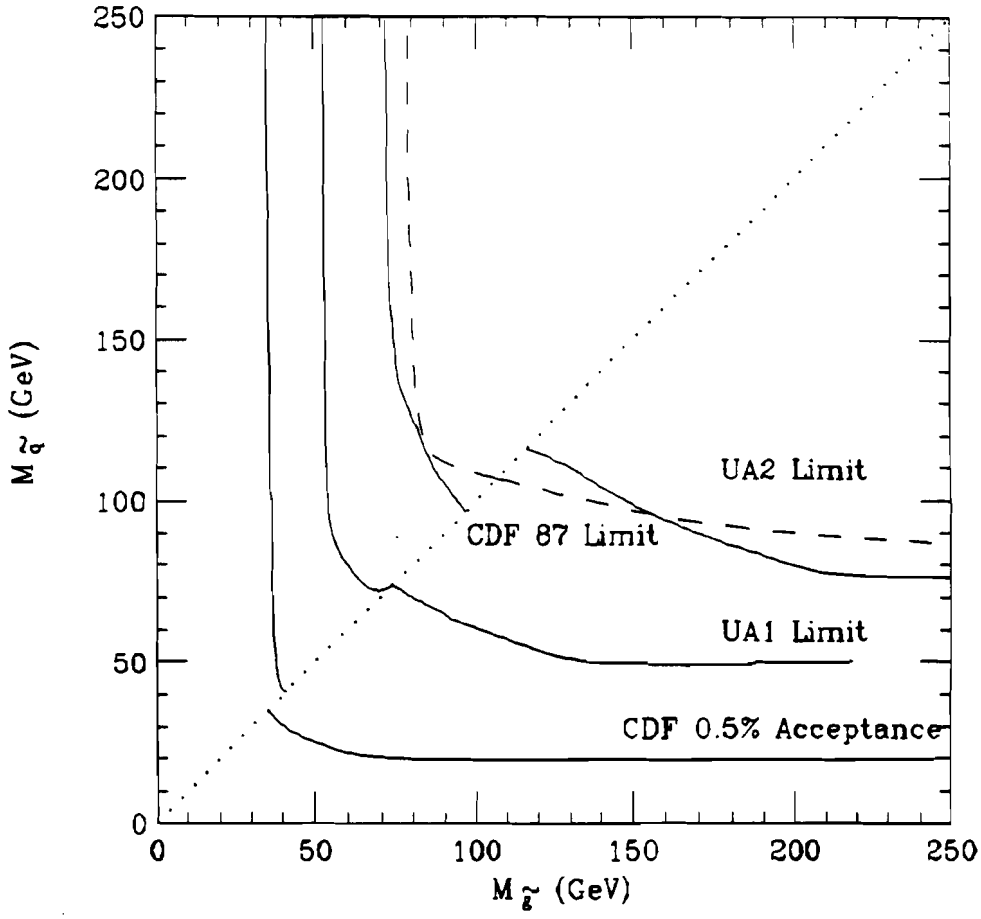

Figure 2.6: Squark and gluino mass limits from previous experiments.

Chapter 3

Experiment Apparatus and Particle Detection

3.1 Tevatron

The Tevatron is a superconducting accelerator at the Fermi National Accelerator Laboratory. It is located in a circular tunnel with the radius of 1 kilometer. The layout is shown in Figure 3.1.

The beam begins from a Cockcroft-Walton pre-accelerator which accelerates H^- ions to 0.75 MeV. And the Linear accelerator further accelerates them to 200 MeV. Then they are injected into the booster (a rapid cycling synchrotron) and two electrons are removed from the H^- by a thin foil. The protons are accelerated to 8 GeV in the booster before they are injected into main ring (a conventional magnet synchrotron). They are further accelerated to 150 GeV in the main ring. Then the protons are injected into Tevatron in which the magnets have superconducting coils.

Antiprotons($\bar{p}$'s) are produced by extracting the proton beam from the main ring to hit a target. Then the antiprotons produced in the target are accumulated in the $\bar{p}$ accumulator which actually has two rings. One is for debunching in which a rotation in synchrotron phase space is done to reduce the energy spread at the cost of increasing the time spread of the $\bar{p}$ bunch. After debunching, the $\bar{p}$'s are added to the circulating beam in the accumulator where stochastic cooling takes place to reduce the random motions of the $\bar{p}$'s: horizontal, vertical and in synchrotron phase space.

In the collider run, protons and antiprotons are injected into Tevatron from

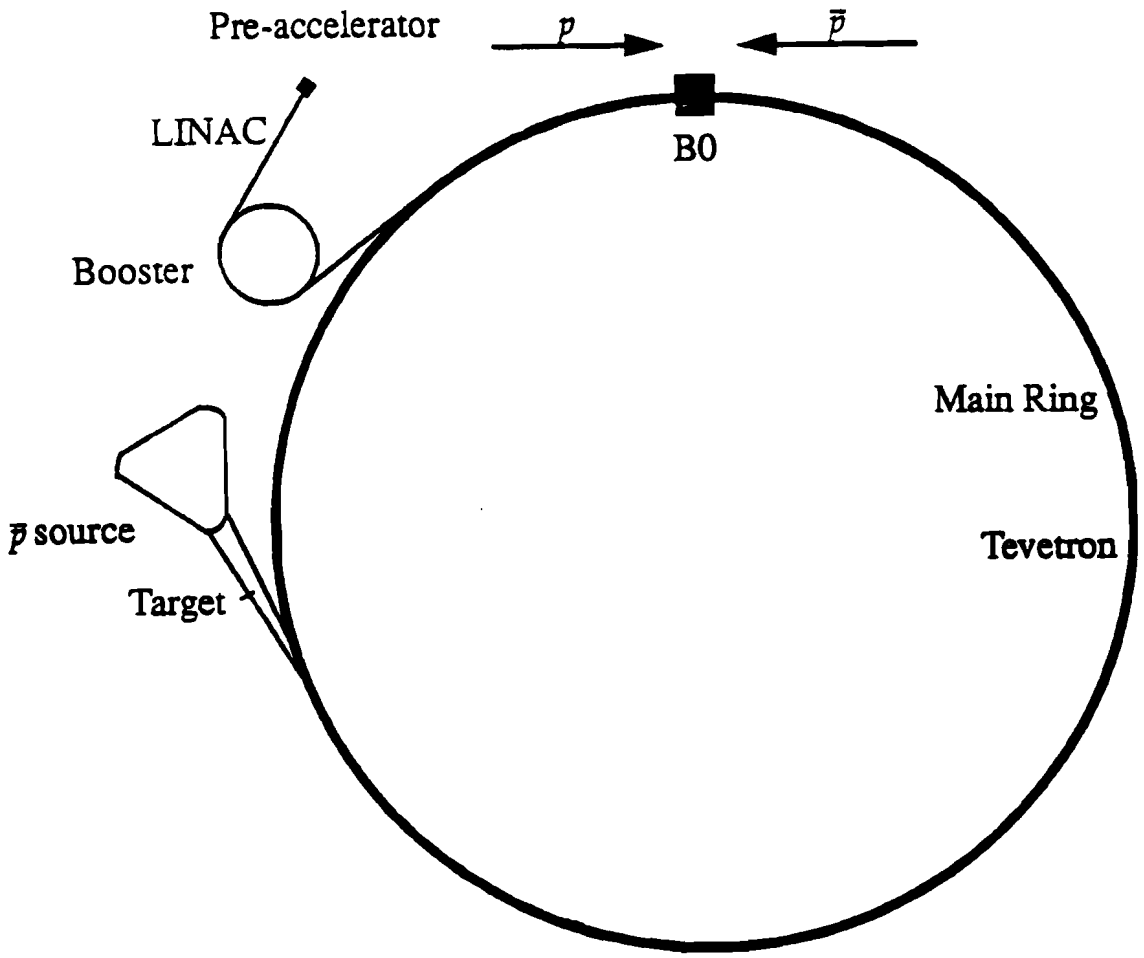

Figure 3.1: Fermilab accelerator complex

opposite directions and accelerated to 900 GeV. Then they collide with each other. This yields the center-of-mass energy of 1.8 TeV.

During most of the 1988-89 run, the Tevatron was run with 6 bunches of protons and 6 bunches of antiprotons. This led to an interval between beam-crossings of about 3.5 μs. The typical luminosity at B0 collision point was 0.5 to $2.0 \times 10^{30} cm^{-2} s^{-1}$.

3.2 Collider Detector at Fermilab

The Collider Detector at Fermilab (CDF) is a general purpose particle detector. It consists of a 2000-ton central detector with the superconducting solenoidal magnet, steel yoke, tracking chambers, electromagnetic calorimeters, hadron calorimeters and muon chambers, and two identical forward/backward detectors with segmented time-of-flight counters, electromagnetic calorimeters, hadron calorimeters and muon toroidal spectrometers. The central detector can be rolled out of the collision hall for maintenance and upgrade during non-collider operation.

The major function of this detector is to measure the energy, momentum, and, where possible, the identity, of the particles produced during the proton-antiproton collision.

A brief description to the components related to this thesis is given below. The detailed description of the individual detector component can be found in various papers [32]-[57]. Figure 3.3 shows the CDF detector.

In the detector coordinate system commonly used at CDF, we choose z axis along the proton beam direction (East) with zero at the detector center, y axis upward and x axis towards outside of the Tevatron ring (North). We use R as the distance to the beam line in cylindrical coordinates; ϕ is the azimuthal angle, and θ is the polar angle relative to the positive z-axis in spherical coordinates. In

practice we also use pseudorapidity which is defined as

$$\eta = -\ln \tan \frac{\theta}{2}.$$

In this thesis the word "electron" usually means both electron and positron. Muon (μ), τ lepton and quark also refer to both the particles and their antiparticles.

3.2.1 Trigger Counters and Luminosity Monitoring

The beam-beam counters (BBC) are a plane of scintillation counters on the front of each forward/backward electromagnetic calorimeter. The counters are arranged in a rectangle around the beam pipe. They cover the angular region from 0.32° to 4.47°. The BBC provide a "minimum-bias" trigger for the detector. and are also used as the primary luminosity monitor.

3.2.2 Vertex Time Projection Chamber

The vertex time projection chamber (VTPC) consists of eight dual time projection chambers surrounding the beam pipe. Its major function is to provide determination of the z-position of the primary interaction vertex (or vertices).

A study of a data sample collected during 1987 run shows that the uncertainty of the reconstructed vertex z position is about ± 0.3 cm.

3.2.3 Central Tracking Chamber

The central tracking chamber (CTC) is a wire chamber with 84 layers of sense wires arranged into 9 superlayers. It is located inside the superconducting solenoid as shown in Figure 3.2.

The CTC information can be used to determine single charged particle momenta. This has been used in the online triggering as well as the offline analysis.

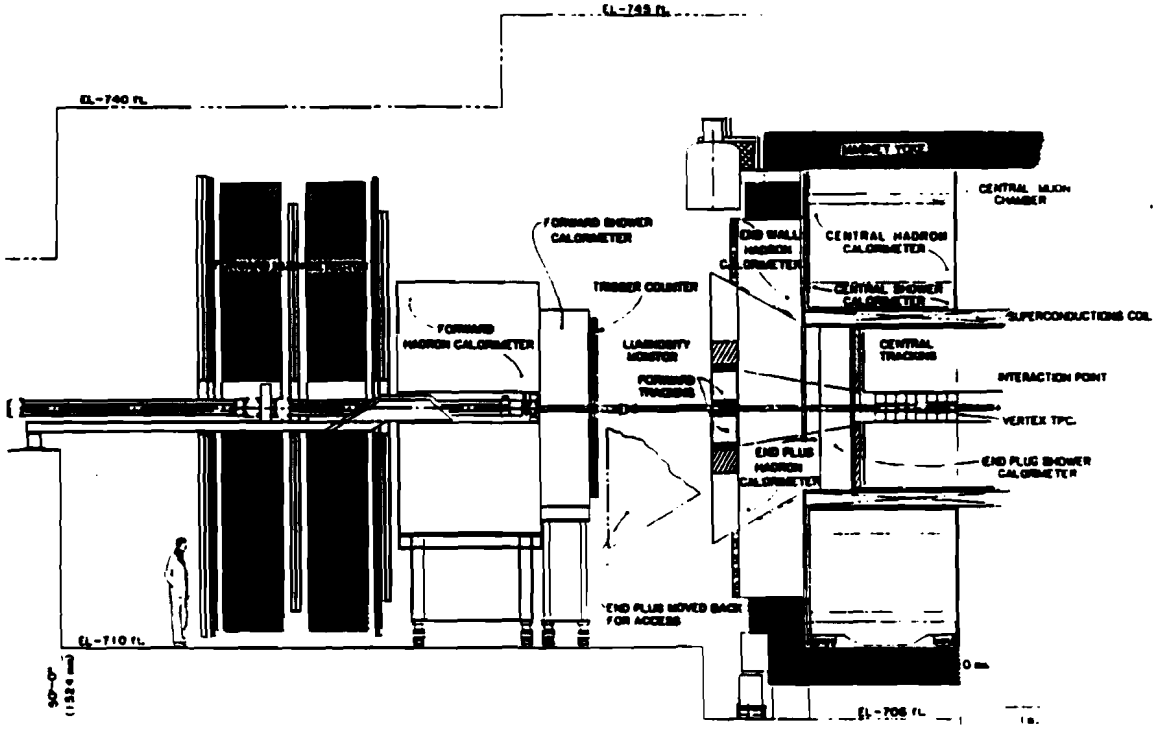

Figure 3.2: Cross section through a vertical plane of one half the CDF detector. The detector is symmetric about the midplane and roughly symmetric around the beam axis.

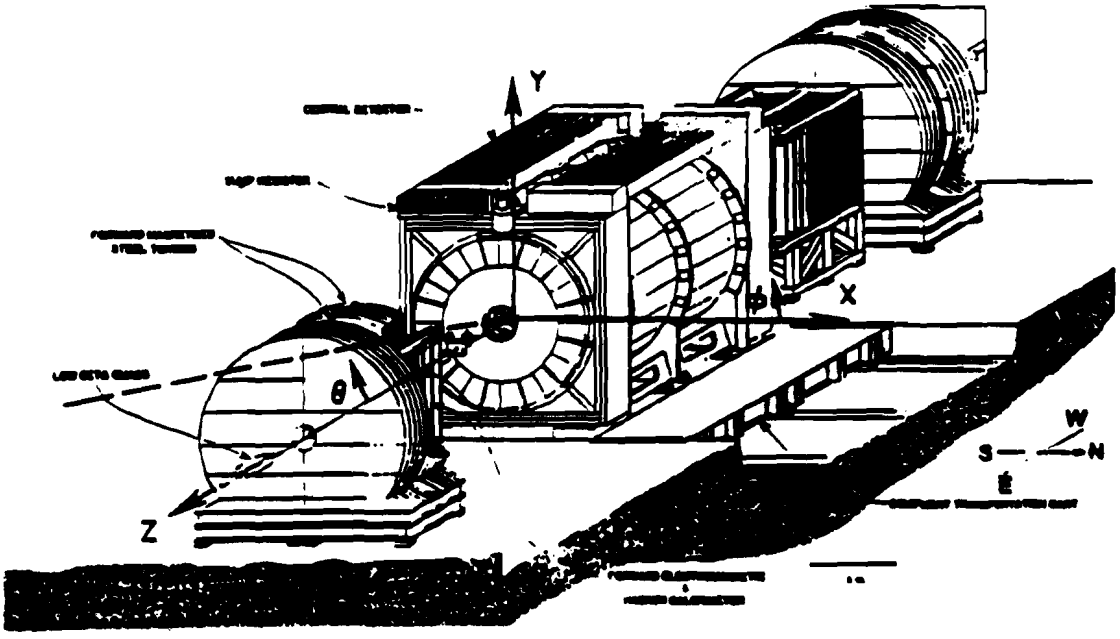

Figure 3.3: CDF detector

The transverse momentum resolution $dP_T/P_T < 0.0017P_T$ GeV/c in $|\eta| < 1.0$.

3.2.4 Superconducting Solenoid Magnet Coil

The superconducting solenoid magnet coil is made of an aluminum-stabilized NbTi/Cu superconductor. During the 1988-89 run it provided a uniform 1.41 T magnetic field along the incident beam direction in the CTC region.

3.2.5 Calorimeters

The CDF calorimeters consist of several parts: central electromagnetic calorimeter, central hadron calorimeter, end wall hadron calorimeter, end plug electromagnetic calorimeter, end plug hadron calorimeter, forward electromagnetic calorimeter and forward hadron calorimeter. They are all shown in Figure 3.2.

Central Electromagnetic Calorimeter

The central electromagnetic calorimeter uses a hybrid design. It consists of the lead and scintillator layers with an embedded strip chamber approximately at the depth of maximum particle multiplicity for electromagnetic showers. The scintillator provides a good energy resolution and the strip chamber provides the position determination and transverse development at the shower maximum.

The average energy resolution of the central electromagnetic calorimeter $\sigma(E)/E$ is $13.5\%/\sqrt{E\sin\theta}$ (E in GeV).

Central and Endwall Hadron Calorimeter

The central and endwall hadron calorimeters are made of steel and scintillator. The central calorimeter has 32 layers with 2.5 cm sampling and the endwall calorimeter has 15 layers with 5.0 cm sampling.

The energy resolutions are shown in Figure 3.4.

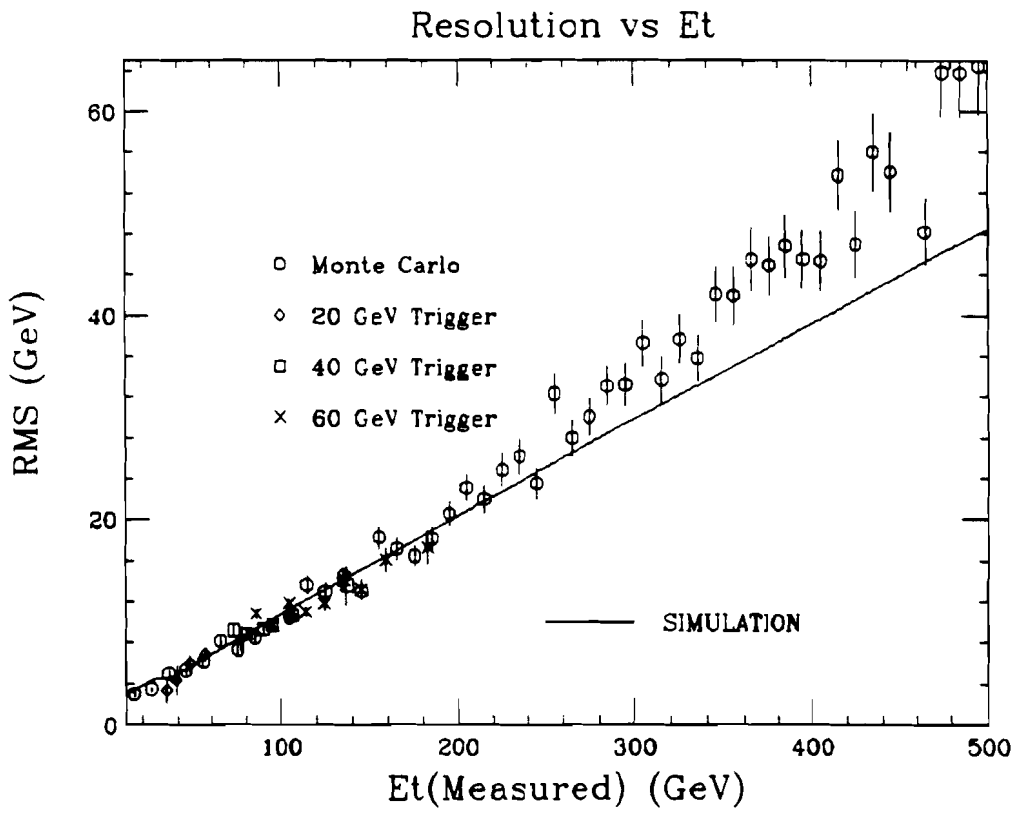

Figure 3.4: Energy resolutions of central and endwall hadron calorimeters

End Plug Electromagnetic Calorimeter

The end plug electromagnetic calorimeter covers both ends of the superconducting magnet coil. Each of them are made of four quadrants of $\delta\phi = 90^{\circ}$. And each of the quadrants consists of 34 layers of proportional tube arrays interleaved with 2.7 mm thick lead absorber panel filling about 50 cm in depth.

End Plug Hadron Calorimeter

The end plug hadron calorimeter shown in Figure 3.2 has 20 layers of steel and proportional tubes.

Forward Electromagnetic Calorimeter

The forward electromagnetic calorimeter consists of 30 sampling layers of proportional tube chambers with cathode pad readout separated by lead sheets for a total thickness of 25.5 radiation lengths. The measured energy response of the calorimeter is linear up to 160 GeV, and the measured energy resolution, σ_E/E, is approximately $25\%/\sqrt{E}+0.5\%$.

Forward Hadron Calorimeter

The forward hadron calorimeter is composed of proportional tube chambers and steel plates. It covers a pseudorapidity region of $2.2 \leq |\eta| \leq 4.2$.

A summary of the calorimeter properties is shown in Table 3.1.

3.2.6 Central Muon Chamber

The central muon system covers a pseudorapidity region of $|y| \leq 0.7$. It is made of drift chambers operating in limited stream mode. It identifies muons by their penetration of the 4.9 absorption length of the central calorimeter, measures

	Central		Endwall	Endplug		Forward	
	EM	Hadron	Hadron	EM	Hadron	EM	Hadron
η	0-1.1	0-0.9	0.7-1.3	1.1-2.4	1.3-2.4	2.2-4.2	2.3-4.2
Medium	p.s.*	a.s.†	a.s.†	proportional tube chambers with cathode pad readout			
Absorber	Pb	Fe	Fe	Pb	Fe	94%Pb, 6%Sb	Fe
Thickness	0.32	2.5	5.1	0.27	5.1	0.48	5.1
# of Layers	31	32	15	34	20	30	27
$\sigma_E/E(\%)$	2	11	14	4	20	4	20
$\Delta x \times \Delta y(\mathrm{cm}^2)$	0.2×0.2	10×5	10×5	0.2×0.2	2×2	0.2×0.2	3×3

* p.s.: polystyrene scintillator, † a.s.: acrylic scintillator.

Table 3.1: CDF calorimeter performance

their positions and directions, and provides a Level 1 trigger for muons which have a transverse momentum greater than a given set value.

3.2.7 Level 0, Level 1 and Level 2 Trigger System

A three-level fastbus based trigger system was used in 1988-89 run. Its purpose was to reduce the event rate and select the most interesting events. The interaction rate was about 50 kHz at luminosity of $1 \times 10^{30} cm^{-2} s^{-1}$. The trigger rate out of Level 2 was 5 Hz or less with about 10% deadtime.

The following is a brief description of the each subsystem.

Level 0

The Level 0 trigger was implemented in the early stages of 1988-89 run. It is a beam-beam counter trigger employing high speed coincidence logic. It requires that both the East and West counters have hits during a beam crossing. Its decision is made in less than 0.5 μs.

When a Level 0 trigger is detected, the sample-and-hold circuits are activated to store on capacitors the analog information from each of detector channels.

Level 1

The Level 1 decision is based on the global energy deposition in the calorimeter and the information from muon chambers. Fast outputs from the front end calorimeter sample-and-hold circuits are input to summing and comparator circuits. With hybrid analog/digital circuits fast multiplication and sums are done to compute ΣE, $\Sigma E_T = \Sigma E \sin\theta$, $\Sigma E_x = \Sigma E_T \cos\phi$ and $\Sigma E_y = \Sigma E_T \sin\phi$ for EM and hadron calorimeters. From these quantities one can calculate event's total E_T and $\not{E}_T$. There are a few types of triggers in Level 1: jet, central electron, photon and muons. It completes its decision in about 5 μs, and if it is not satisfied, the analog information previously stored is zeroed and the front end circuits are re-activated for the next beam crossing.

Level 2

The Level 2 is more sophisticated than Level 1 but requires more time, typically about 40 μs. It has the cluster finder processor and has the information from CTC fast tracker. So that it can make better identification on electron, muon and photon events. It also has better recognition for jet events, and it can apply combinations of requirements such as $\not{E}_T$ and jet E_T .

When Level 2 is satisfied, the analog signal are digitized and collected by the data acquisition system (DAQ) for subsequent analysis.

3.2.8 Data Acquisition System

The CDF data acquisition system uses a multilevel FASTBUS network. At the lowest level, scanners (called MEP/MX and SSP) read and buffer data from

RABBIT (Redundant Analog Bus-Based Information Transfer) crates containing analog-to-digital converters (ADC's) from calorimeters, and FASTBUS front end system containing time-to-digital converters (TDC's) from tracking chambers. Operations of these front end scanners are coordinated by the Trigger Supervisor module which initiates parallel readout after receiving Level 1 and Level 2 triggers. The data flow after scanners is supervised by the Buffer Manager. It directs the Event Builder to collect and format data from a set of scanners, and push the formatted data into one of the Level 3 nodes. The Level 3 node processes the event and the Buffer Multiplexor reads the event out of Level 3 and puts it on VAX memory where the Tape Logger may copy it to tapes, and other consumer processes may read it and analyse it for online monitoring. Figure 3.5 shows the data flow in the data acquisition system.

3.2.9 Level 3

Level 3 is a VME based microprocessor farm. Each of the 58 processor boards has a Motarola 68020 CPU with 68021 floating point coprocessor and 6 MBytes of memory. It can run the FORTRAN program and to make more accurate trigger decision for the events based on algorithm developed offline.

In the 1988-89 run, Level 3 performed two major functions: first, reformatting the TDC data; second, running the trigger algorithm and setting trigger bits to classify events.

The Level 3 $\not{E}_T$ trigger was based on the information from all calorimeters. It used the same algorithm as offline to reconstruct the energy deposition in the calorimeter, to remove electronic noise and to correct for the large signals induced by low energy neutrons.

Level 3 also had a fast algorithm to reconstruct tracks based on CTC information which were very useful for lepton triggers. These results were also used by some offline programs as stated in later chapters.

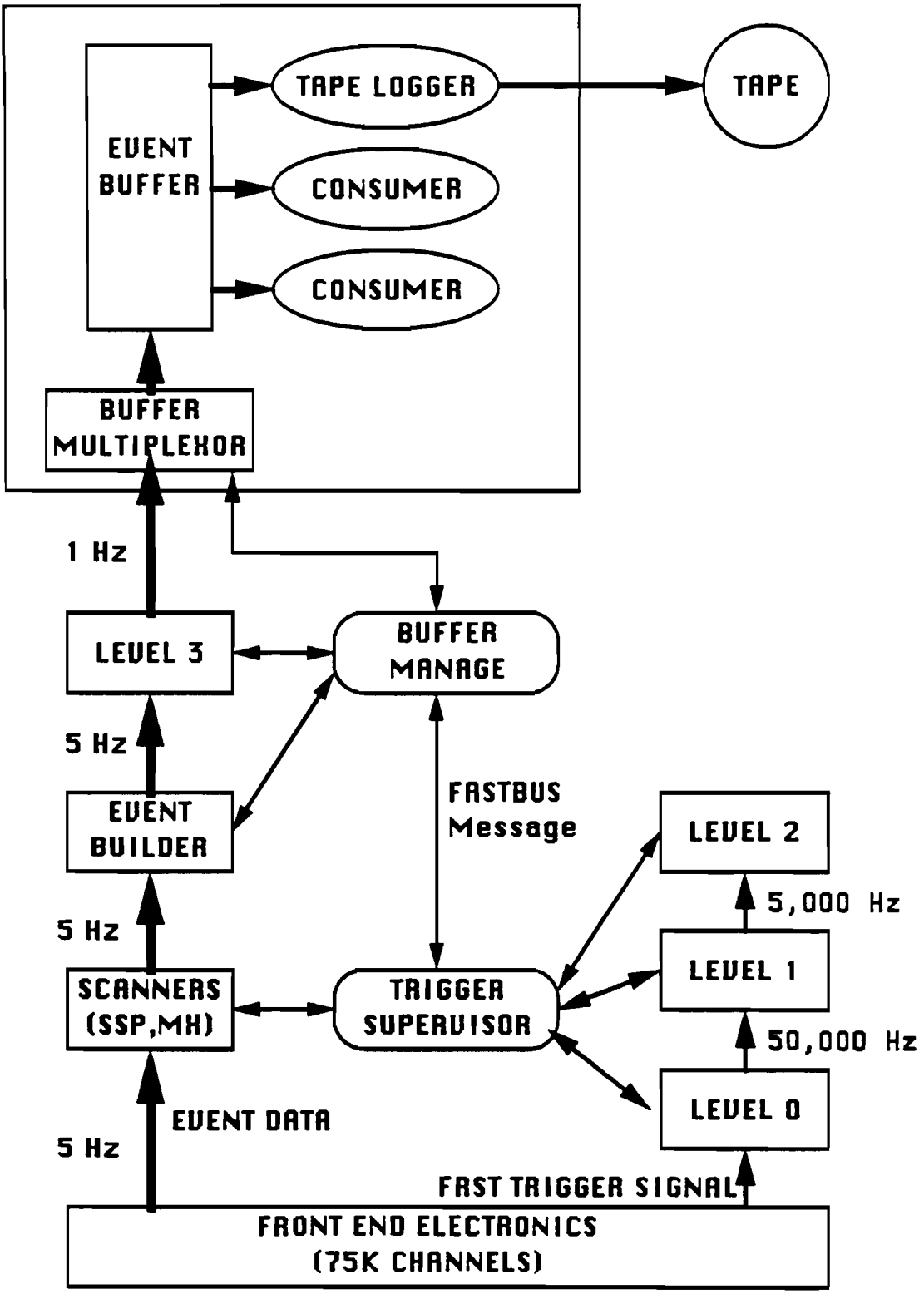

Figure 3.5: Data flow in the CDF data acquisition system

3.3 Trigger and Data Collection

3.3.1 Trigger

The analysis reported in this thesis is based on the data collected with the online $\not{E}_T$ triggers. As previous discussed, CDF had a 4-level online trigger system in 1988-1989 run. No $\not{E}_T$ condition were imposed in Level 0 and Level 1. It was selected by Level 2 and Level 3.

Level 2 $\not{E}_T$ Trigger

The Level 2 $\not{E}_T$ trigger requires the following:

A The transverse energy imbalance ($\not{E}_T$) of all calorimeter components is greater than 25 GeV (in practice the cut is $(\sum E_x)^2 + (\sum E_y)^2 > 625\text{GeV}^2$).

B The leading calorimeter cluster has at least 6 GeV energy deposited in electromagnetic calorimeters.

C The leading calorimeter cluster has no seed tower in forward calorimeters.

The requirement **B** and **C** are imposed to reject the events caused by "Texas Towers" (the calorimeter response to the low energy neutrons). The requirement **B** also helps reject cosmic ray events.

Level 3 $\not{E}_T$ Trigger

The Level 3 trigger has an algorithm similar to that of the offline analysis program. It requires

A The $\not{E}_T$ after calorimeter cleanup is greater than 15 GeV.

B If the event has a jet with $E_T \geq 10$ GeV which is within 30° opposite to the leading jet direction in ϕ, then the $\not{E}_T$ after cleanup must be ≥ 40 GeV.

The major function of Level 3 in 1988-89 run was to improve the data quality. So its $\not{E}_T$ threshold was actually lower than that of Level 2. The requirement **B** is to reject dijet events which appear to have $\not{E}_T$ because of energy mismeasurement.

3.3.2 Data Collection

The data sample used in this thesis was collected during the 1988-89 run. A number of calibrations and stability checks were performed regularly during the run.

- The gain of the gas calorimeters was monitored continuously by a "Gas Gain" program. The gain was a function of temperature and pressure, and new constants were downloaded if it differed more than 3% from the previous value. The new constants were also downloaded each time when a run started normally.
- The gains of scintillation calorimeters were checked approximately once a day by a short run with light pulsers. Gains were also measured by the response to a Cs^{137} (or Co^{60}) radiation source which could be moved into various position in the calorimeter array.
- The trigger was calibrated by a calibration once a day.
- The hot channels were masked out from trigger when it caused a large amount of change of the trigger rate. Otherwise they were masked during the regular calibration run. The hot/dead channels' information were recorded in the database for every run in order to make offline correction.
- Pedestals were checked once a day by a calibration run.

The uncertainties relevant to this study are $\pm 3\%$ in gas gain and $\pm 0.4\%$ in scintillation calorimeter gain. Although there was uncertainty in trigger thresholds, software cuts described in next chapter eliminated the source of uncertainty.

During a number of runs part of the gas calorimeters were off for various reasons. Such runs were not used in this analysis.

Chapter 4
Data Analysis: Event Selection

There are two ways to search for new particles. The first one is to look for new phenomena which cannot occur with known particles. This is the best way to pursue the search if the new particle has some very distinctive characteristics. However this is not the case for $\tilde{q}$ and $\tilde{g}$. So the second method was used in this study: to look for events with certain characteristics at rates higher than expected from known particles, *i.e.* to look for a signal on top of a background from conventional processes. If the background contribution in these events can be predicted precisely, then possible excess events due to the existence of the new particle can be measured and their significance evaluated.

The distinctive signature for $\tilde{q}$ and $\tilde{g}$ is large $\not{E}_T$ in purely hadronic events. So the strategy will be to isolate a sample of such events in the data, to study their distribution as a function of $\not{E}_T$, to calculate the distribution from conventional processes and from SUSY particles, and finally, to assess the statistical significance of any possible SUSY contribution.

As discussed before CDF is a general purposed detector, so the raw data contains all kinds of events. The raw data tapes are usually first processed by a production pass to generate different data summary tapes (DST's) for different kind of events. Most physics analyses then start from these DST's.

This chapter first gives a description of the production data analysis, and then a description of the analysis specific to this study. At each stage certain cuts were applied to the data to select the events with better quality (signal-to-background ratio). Initially they concentrated on event quality and elimination of spurious

events. At later stage, they focused on specific physics and rejecting events due to other processes. Detailed discussion of the precise tuning for each of these cuts is beyond the scope of this thesis. References to CDF technical notes on these topics are provided for interested readers. A summary of all cuts applied from triggering to final SUSY selection is presented in Table 4.1.

4.1 Spin Cycle and Production

The raw data tapes collected in 1988-89 run were first processed through a process called Spin Cycle. The output tapes from Spin Cycle were later processed through production pass.

4.1.1 Spin Cycle

In the spin cycle partial event reconstruction was done, and the events passed certain selection criteria (see Appendix B) were saved to the output tapes.

The event reconstruction in the spin cycle was based on the raw data from calorimeters, muon chambers, VTPC and BBC. But instead of doing the full CTC tracking reconstruction, it simply used the online reconstructed CTC tracks.

4.1.2 Spin Production

The output tapes from spin cycle were further processed with the full production analysis package. It contained the full CTC tracking reconstruction and the best calibration constants.

There were four output streams from the production based on the different selection criteria for the different physics purpose. They were QCD, EWK(electroweak), TOP(top search) and MET ($\not{E}_T$) tapes. In this analysis we only used the MET tapes. The selections for MET stream were as the following:

Data Path and Analysis Stage	Operation	Cuts
Level 2	$\not{E}_T$ selection	$\not{E}_T \geq 25$ GeV etc. as discussed before
Front End Scanners	Pedestal/Gain Correction	channels with ADC counts below threshold did not read out
Event Builder	Organizing Events into YBOS Format	
Level 3	Calorimeter Cleanup. Calculating $\not{E}_T$. Clustering and 2-D Tracking	Dijet cuts etc. as discussed before
Spin Cycle	Partial Event Reconstruction and Fast Event Selection	Appendix B
Production	Full Event Reconstruction and $\not{E}_T$ Selection	$\not{E}_T \geq 20$ GeV and dijet rejection etc. discussed in the text
Sorting $\not{E}_T$ Events	Selecting Events with $\not{E}_T$ and Two Jets	Rejecting cosmic ray and events from bad runs, 2 jets with $E_T \geq 15$ GeV (see below)
SUSY Selection	Reject Events with e or μ, Select High $\not{E}_T$ events	$\not{E}_T \geq 40$ GeV, rejecting e, μ events, QCD events and events with multiple vertices or vertex off center

Table 4.1: Data path and cuts

- The event has to pass one of the following Level 2 triggers:
  - 60 GeV jet trigger
  - trijet trigger
  - total E_T triggers
  - total EM E_T triggers
  - 12 GeV electron triggers
  - photon triggers
  - $\not{E}_T$ triggers
- The event had to have the good data structure. In other words there was no detector and readout system malfunction.

  The event had no more than 8 GeV energy deposited in the central hadron calorimeter out of the beam crossing time window. This rejected most of the cosmic ray events.
- The $\not{E}_T$ selection had the following requirements:
  - $\not{E}_T > 20$ GeV
  - $\sigma \equiv \frac{\not{E}_T}{\Sigma E_T} > 2.4$
  - The leading jet cluster was required to be in the good detector region ($|\eta| < 3.5$), and to have at least 5% of its energy deposited in the electromagnetic calorimeters.
  - If the event had a jet cluster with $E_T > 5$ GeV within 30° opposite to the leading jet cluster in ϕ direction, the event was removed from the data set.

The last two requirements in $\not{E}_T$ selection are proposed to reject events with fake $\not{E}_T$ due to detector response. It has been discussed in other papers [58,29].

4.2 Further Selection on $\not\!\!E_T$ Events

The output tapes from spin production were further processed by $\not\!\!E_T$ analysis group and the events were classified into four categories and written to the different tapes. They were CWS(central W decays to electron and electron neutrino), MMU(muon events), MON(monojet events) and ZEN(events with at least two jets). We only used ZEN events in this thesis.

Before the events were classified, they all had to satisfy the following requirements.

- Events from bad runs were rejected.
- In order to eliminate cosmic rays, an event was rejected unless it had at least one jet cluster in central detector region with charge fraction CHR > 0.1.

The charge fraction of a jet is defined as the ratio of the scalar sum of all charged particles' momenta (measured from CTC) to the jet cluster energy.

At the next level of event selection, the ZEN filter algorithm required

- $\not\!\!E_T \geq 20$ GeV
- Events have at least 2 jet clusters with $E_T > 15$GeV, EMF ≥ 0.1, $|\eta| < 3.5$,

where EMF is the ratio of the energy deposited in electromagnetic calorimeter to the total cluster energy.

These cuts were discussed in References [59,60].

4.3 SUSY Selection

We applied the following cuts to events which passed the ZEN filter to select events for SUSY analysis. Some of these are redundant with cuts applied at earlier stages of the analysis.

- $\not{E}_T \geq 40$GeV.
- $\sigma \geq 2.8$
- Events were required to have at least one jet cluster with
  - $E_T > 15$GeV,
  - $|\eta| < 1.0$,
  - CHR > 0.2,
  - $0.1<$EMF<0.9,

  where CHR $= P_T(\text{charge})/E_T$ is the charge fraction of the jet, $P_T(\text{charge})$ is the sum of the transverse momenta of all CTC tracks associated with the jet cluster.
- The "two good jet clusters" requirement was tightened to require $0.1<$EMF<0.9.
- Events with an electron candidate were rejected if there was a jet cluster with
  - $E_T > 15$ GeV,
  - EMF > 0.9.
- Events with a muon candidate with $P_t > 15$GeV were rejected. A muon candidate is defined as one of the following: a) in central muon chamber covered region, a good muon chamber hit which matches with a CTC track and has a small amount of energy deposited in the matching calorimeter tower; b) outside of central muon chamber covered region, a central minimum ionized track determined from CTC measurement which matches the calorimeter tower with a small amount of energy deposition. In both case, the energy deposited in the calorimeter towers matching the CTC track (R

$\equiv \sqrt{(\Delta\eta)^2 - (\Delta\phi)^2} < 0.13$) should have $E_{EM} < 2.0\text{GeV}$, $E_{had} < 6.0\text{GeV}$ and $E_{EM} - E_{had} > 1.0\text{GeV}$.

- Events were rejected if they had any jet cluster with a) $E_t > 15$ GeV, b) $|\phi_{jet} - \phi_{\not{E}_T}| < 30°$. This requirement removed trijet events with the $\not{E}_T$ caused by mismeasurement of one of jet energy, and some $b\bar{b}$ events in which b or $\bar{b}$ decayed into leptons. Figure 4.1 shows the angle between the third jet and $\not{E}_T$ in the plane perpendicular to the $\bar{p}p$ beams before this cut.

- Events with two or more primary vertices, *i.e.* two independent $\bar{p}p$ collisions in the same crossing, were removed from the data set. $\not{E}_T$ is not well-defined for these events and it is difficult to assign individual calorimeter towers or jet clusters to the proper interaction vertex. The events with the vertex z position off detector center by 60 cm or more were also removed because, in these cases, the detector did not cover the sufficient solid angle, as viewed from the interaction vertex, to prevent particles with large E_T from escaping undetected through un-instrumented areas.

After these selections we scanned the remaining events and removed a few which were identified as cosmic ray events, beam-gas events, and the events with readout problem or a lot of electronic noise. We also required the events to pass the Level 2 $\not{E}_T$ trigger. This leads to a final data sample with 97 events which corresponds to a 4.3 pb^{-1} of integrated luminosity.

The $\not{E}_T$ distribution of the final data set is shown in Figure 4.2, and the jet multiplicity is shown in Figure 4.3.

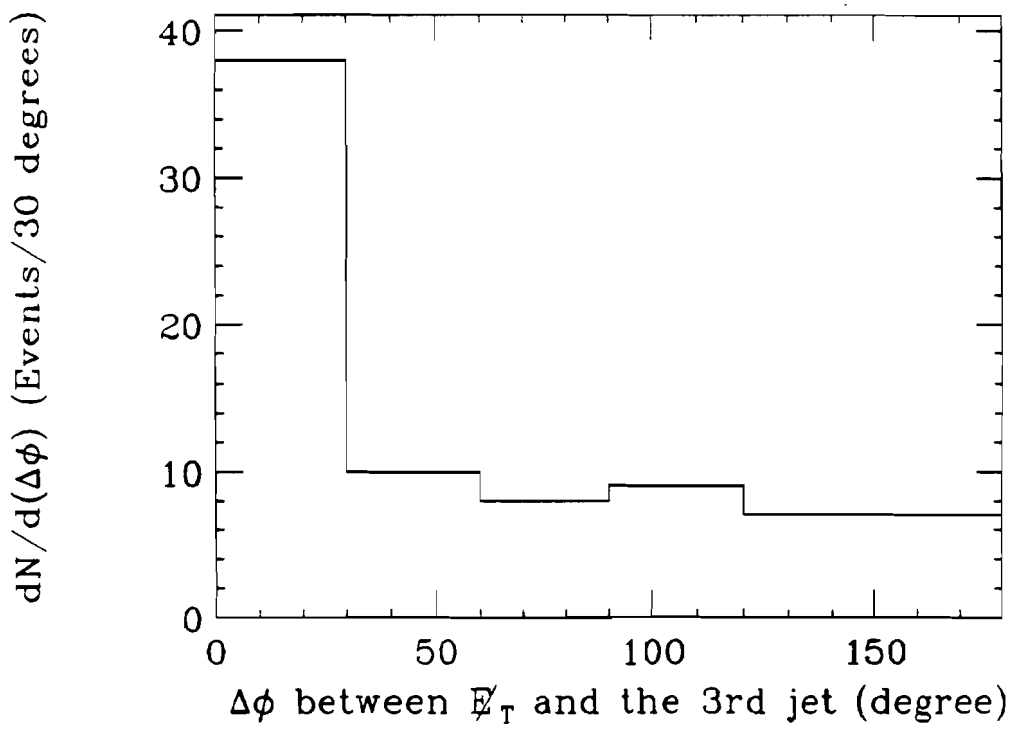

Figure 4.1: $\Delta\phi$ between $\not{E}_T$ and the third jet

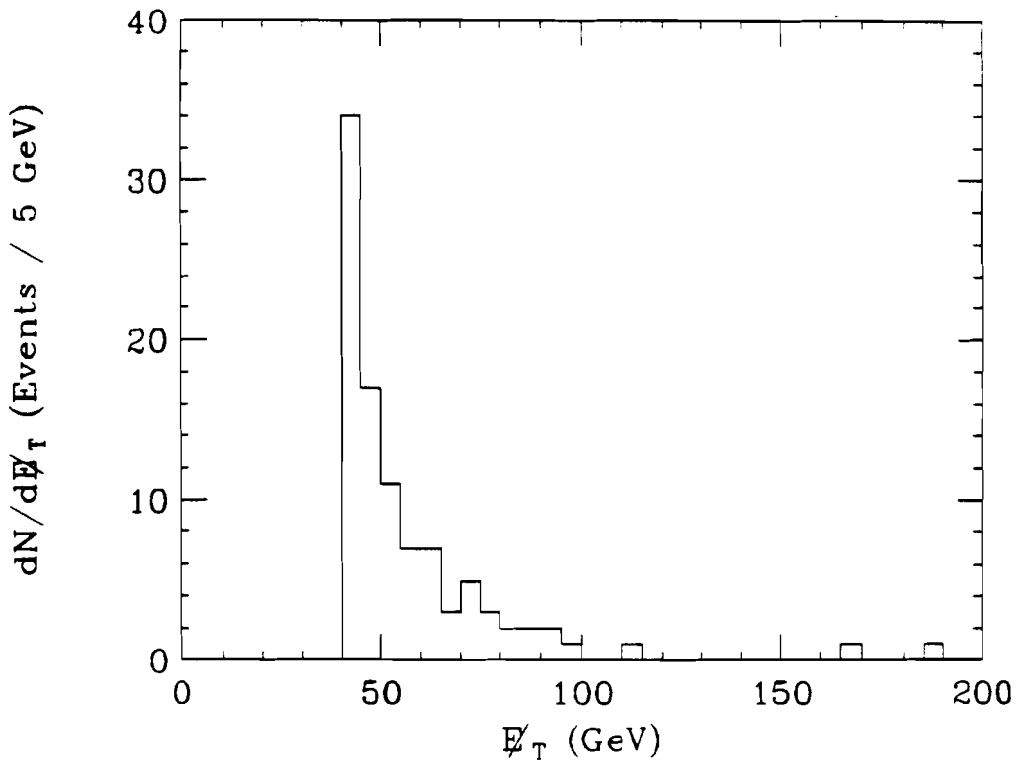

Figure 4.2: $\not{E}_T$ distribution of the selected data sample

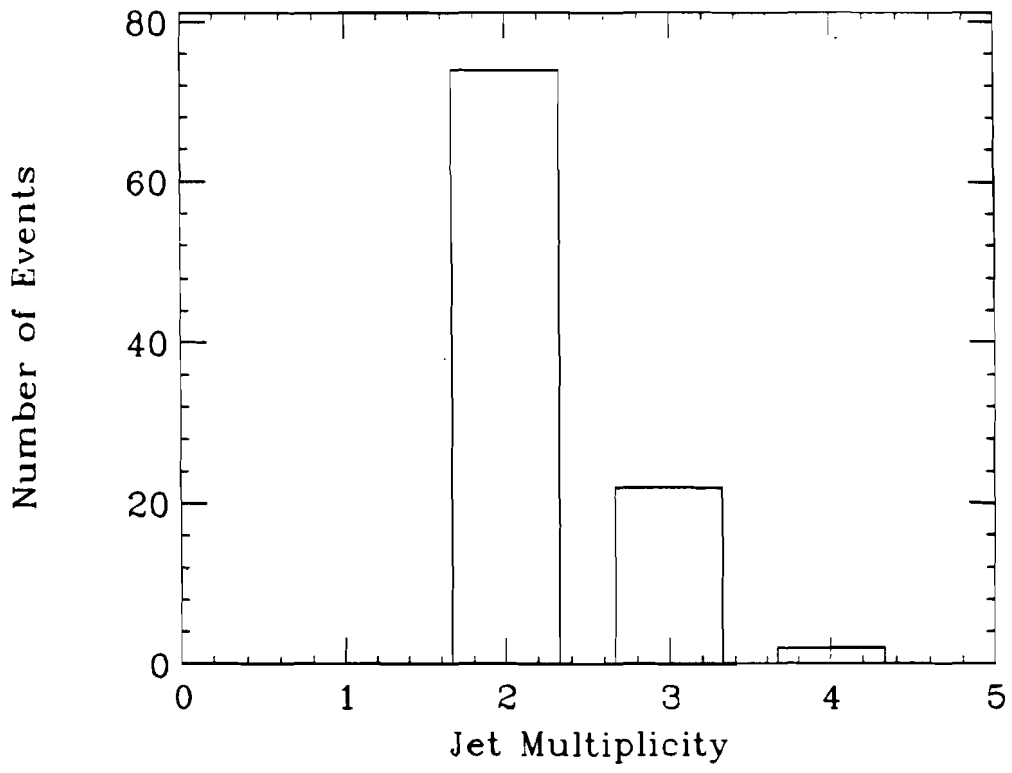

Figure 4.3: Jet multiplicity of the selected data sample

Chapter 5

Data Analysis: Background Study

There are several Standard Model processes which can survive our cuts. In general any processes with a neutrino in the final state can contribute to our background since the neutrino will cause $\not{E}_T$. However, when the $\not{E}_T$ threshold is 40 GeV, the neutrino must to have high P_T in order to generate such high $\not{E}_T$. In this case, the dominant processes are from W(or Z) + jet(s) events as shown in Figure 5.1. Heavy quark events are also a possible background source if the decay is semi-leptonic and the neutrino has high P_T. QCD events can contribute if the jet energy is mismeasured. Other possible background events may come from processes like W(or Z)+γ, W^+W^-, WZ and ZZ, but these processes typically have the production cross section of 1 pb or less so that their contributions are negligible.

For W (or Z) + jet(s) events, when the W (or Z) decay produces a high P_T neutrino it could contribute to background. $Z \rightarrow e^+e^-$, $\mu^+\mu^-$ or $\tau^+\tau^-$ can also cause some $\not{E}_T$ if the lepton goes through an uninstrumented detector region. However the cross section for $\bar{p}p \rightarrow Z \rightarrow e^+e^-$ (as well as $\bar{p}p \rightarrow Z \rightarrow \mu^+\mu^-$ or $\tau^+\tau-$) is 10 times smaller than $\bar{p}p \rightarrow W \rightarrow e\nu_e$ [61], and our cuts are intended to reject events with e or μ, so the contributions from $Z \rightarrow e^+e^-$, $\mu^-\mu^-$ or $\tau^+\tau^-$ small and can be neglected.

To estimate the background, one can use Monte Carlo method to generate events and use detector simulation program to see how many of them will pass the cuts. The other method is to use a control data sample of a certain process, apply cuts to them to see their contributions to backgrounds, or alter the data sample to

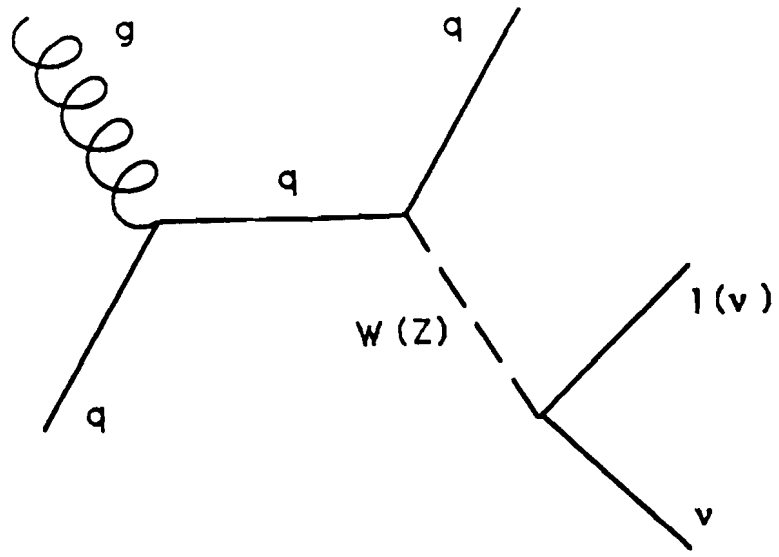

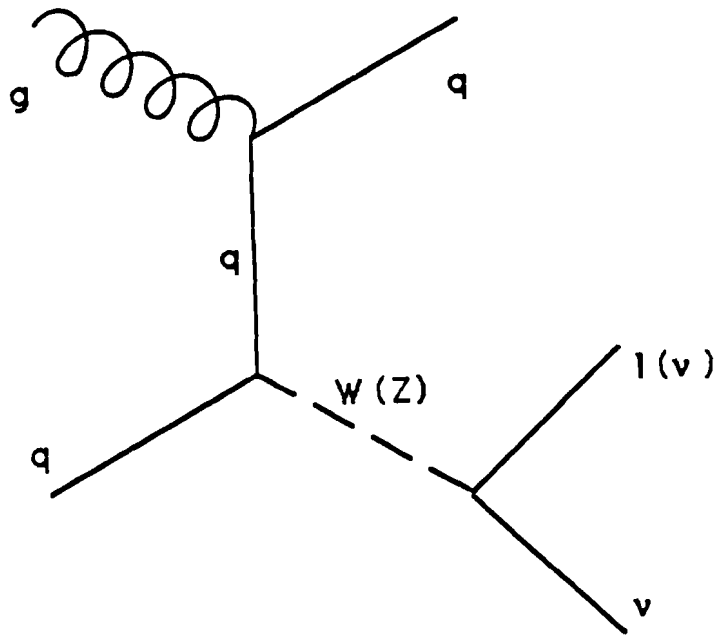

Figure 5.1: W + jet and Z − jet processes from $\bar{p}p$ collision

simulate another processes and apply cuts to see their contributions. In the 1988-89 run, CDF collected a data sample of more than 5000 $W \rightarrow e\nu_e$ events. This enabled us to use them to estimate backgrounds from this sample. Both methods were used to determine backgrounds from $W \rightarrow e\nu_e, W \rightarrow \mu\nu_\mu, W \rightarrow \tau\nu_\tau$ and $Z \rightarrow \nu\bar{\nu}$. The backgrounds from QCD and heavy quark are difficult to estimate in either way. However their contributions are relatively small comparing with W (or Z) – jet(s). We did our best to try to estimate them from our own data sample. In the sections below, we present the number of events and $\not{E}_T$ distributions from specific processes estimated by each of the two methods.

5.1 $W \rightarrow e + \nu$

In $p\bar{p}$ collisions, the W can be produced associated with one or more jet(s). In the case of W + 1 jet, where W decays to e and ν, the neutrino can generate large amount of $\not{E}_T$. If the electron is not isolated or there is other energy deposition in the hadron calorimeter near the electron so that the electron cluster had an EM fraction less than 0.9, the event will not be rejected by the previous cuts. So they contribute to the background.

For W + 2 or more jets, if the electron has low P_T or is lost in detector cracks, the event also contributes to the background.

The STIRLING Monte Carlo [62] and a CDF detector simulation [63,64] program were used to determine the background from W (or Z) – jet(s). Only W (or Z) + 1,2,3 jets events are included in STIRLING Monte Carlo. The $\not{E}_T$ distribution from $W \rightarrow e\nu_e$ events which pass the cuts is shown in Figure 5.2.

From our final data set we found 5 events which were candidates for $W \rightarrow e+\nu$. Four of them had the electron in the central region $|\eta| < 1.0$, the other one had the electron in the end plug region. All five electrons had $E_T > 10$ GeV.

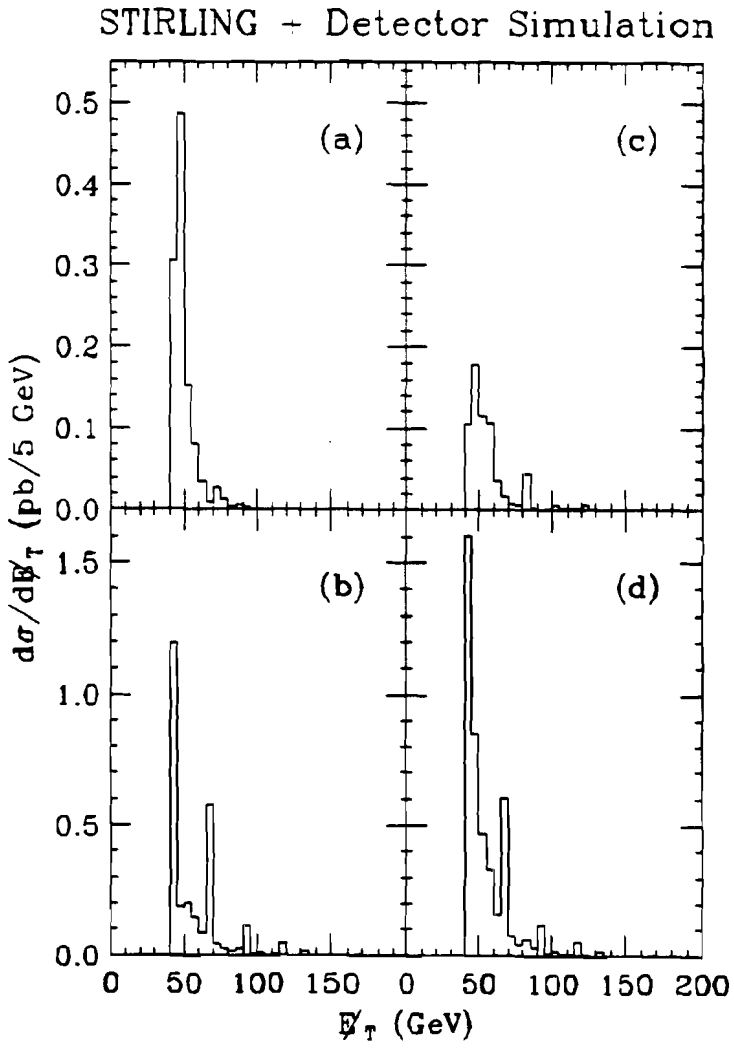

Figure 5.2: Background from Stirling Monte Carlo $W \to e\nu_e$ processes: (a) W + 1 jet, (b) W + 2 jets, (c) W + 3 jets and (d) sum of W + 1,2,3 jets

The electron detection efficiency in the central region is reduced by the detector cracks. The efficiency $\epsilon_{crack} = 0.85 \pm 0.05$ was determined by the study of an inclusive electron data sample.

The total $W \rightarrow e + \nu$ background is obtained by

$$N(W \rightarrow e + \nu) = \frac{1}{\epsilon_e}(\frac{n_c}{\epsilon_{crack}} + n_p).$$

Where $n_c = 4$ is the number of events observed in the central region, and $n_p = 1$ is the number of events observed outside of central detector, $\epsilon_e \equiv \frac{N(E_T>10)}{N(total)}$, $N(total)$ is the number of total $W \rightarrow e + \nu$ events passing the cuts and $N(E_T > 10)$ is the number for those events with electron $E_T > 10$ GeV. From Monte Carlo study we get $\epsilon_e = 0.89 \pm 0.05$. This leads to

$$N(W \rightarrow e + \nu) = 6.4$$

The $\not{E}_T$ distribution is shown in Figure 5.3.

5.2 $W \rightarrow \mu + \nu$

The central muon chambers have limited coverage ($|\eta| < 0.7$). By looking at the minimum ionized track in the CTC (CMIO), we can expand our muon coverage to $|\eta| < 1.2$.

For W + 2 or more jets event, if W decays to a muon which is outside our coverage region, it contributes to the background. Otherwise if the muon has $P_T < 15$ GeV, it also contributes to the background.

The $\not{E}_T$ distribution from STIRLING $W \rightarrow \mu\nu_\mu$ events which pass the cuts is shown in Figure 5.4.

Muons deposit very little energy in the calorimeters. We noted that the muon P_T distribution from W decay is the same as the electron's from $W \rightarrow e + \nu$. Therefore one can simulate the calorimeter response in $W \rightarrow \mu + \nu$ events by

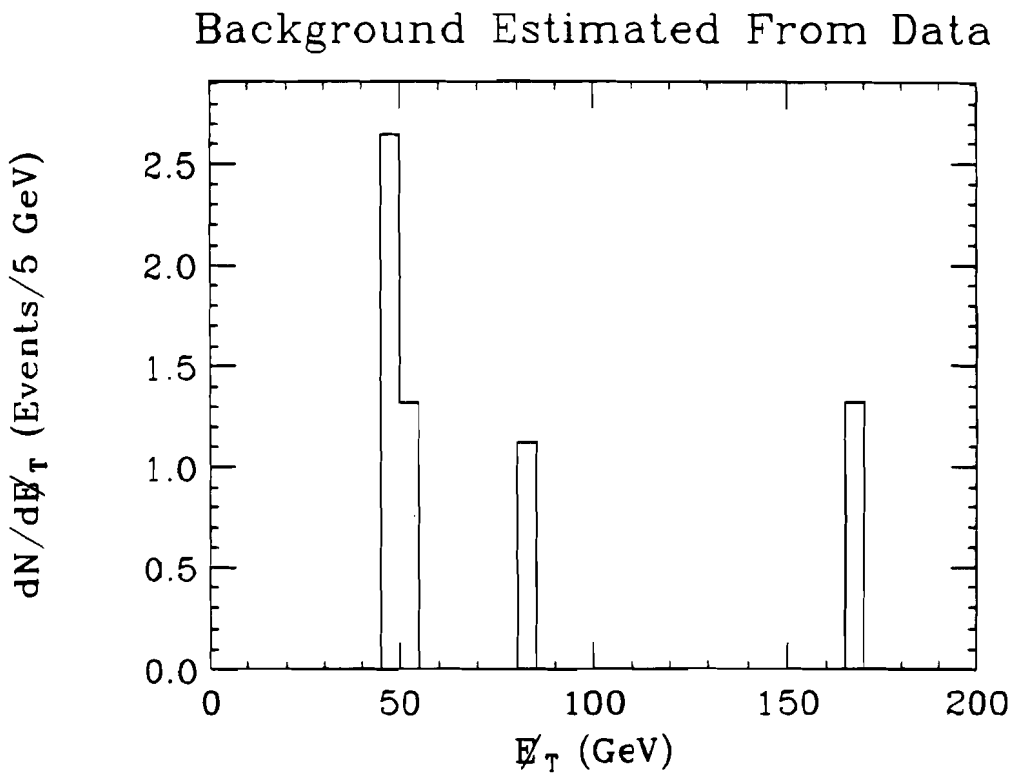

Figure 5.3: Background from $W \rightarrow e\nu_e$ process estimated from data

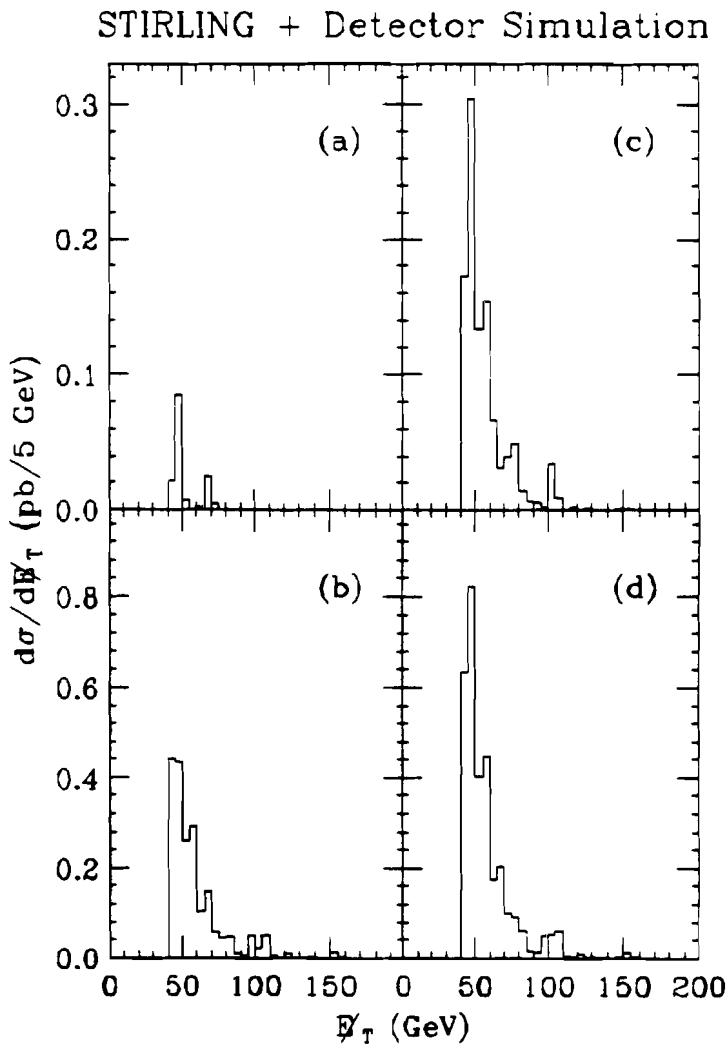

Figure 5.4: Background from Stirling Monte Carlo $W \to \mu\nu_\mu$ processes: (a) W + 1 jet, (b) W + 2 jets, (c) W + 3 jets and (d) sum of W + 1,2,3 jets

removing the energy which electrons deposit in the calorimeters from the $W \rightarrow e + \nu$ events.

The selection for $W \rightarrow e + \nu$ events is discussed in Appendix C. A total of 19 events passed the cuts after the electron energy deposited in calorimeters were removed in these events.

The background contribution from $W \rightarrow \mu + \nu$ is

$$N(W \rightarrow \mu + \nu) = \frac{n_\nu}{\epsilon_{cr}\epsilon_{ele}\epsilon_{el}\epsilon_{M_t}\epsilon_v}(1 - \epsilon_\eta)\epsilon_{trg},$$

where

$\epsilon_{trg} = 0.924 \pm 0.024$ is the $\not{E}_T$ trigger efficiency.

$\epsilon_{el} = 0.97 \pm 0.03$ is the efficiency for $|Q_{ELES}| = 1$, $|Q_{ELES}|$ is the electron charge decided by electron algorithm (this has an implicit requirement of a CTC track matching the calorimeter tower),

$\epsilon_{ele} = 0.83 \pm 0.02$ is the efficiency for the rest of the electron cuts [65],

$\epsilon_{M_t} = 0.96 \pm 0.03$ is the efficiency for transverse mass cut,

$\epsilon_v = 0.47 \pm 0.05$ is the ratio of number of events which have electron $P_T > 15$ GeV, $\not{E}_T > 15$ GeV and $|\eta| < 1.0$, and passed our cuts to the number of total events passed our cuts from $W \rightarrow \mu + \nu$ process,

$\epsilon_\eta = 0.7 \pm 0.05$ is the acceptance for electron with $|\eta| < 1.2$ and $P_T > 15$ GeV.

With $n_\nu = 19$ events and the efficiencies above,

$$N(W \rightarrow \mu + \nu) = 16.6.$$

Their $\not{E}_T$ distribution is shown in Figure 5.5.

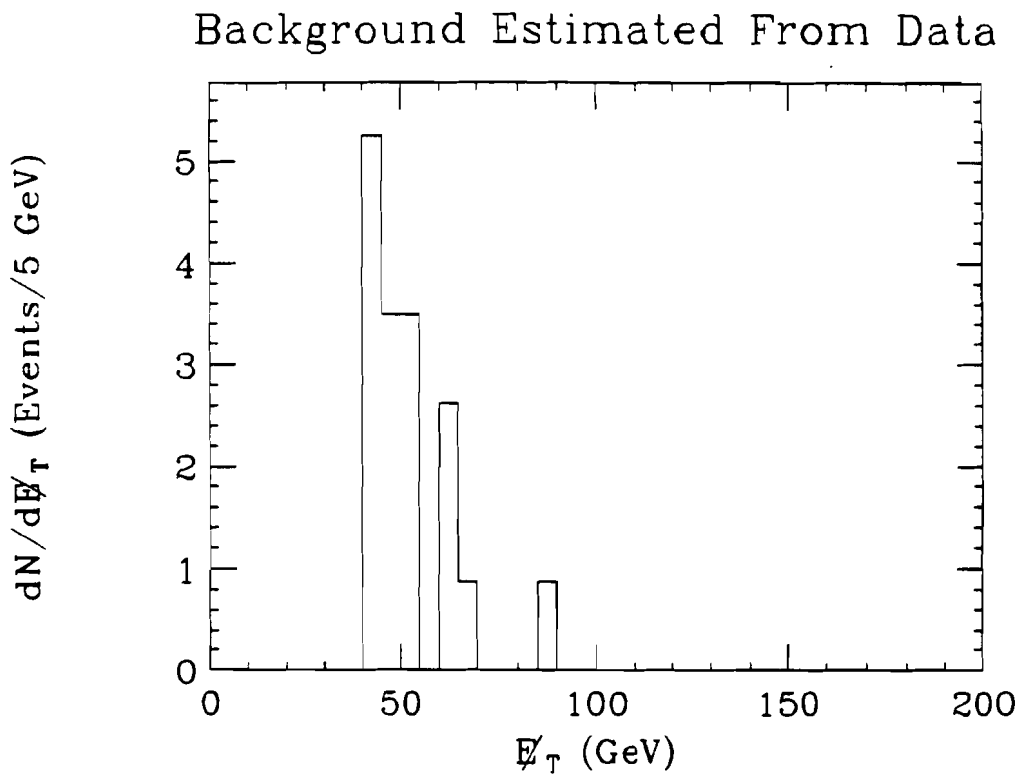

Figure 5.5: Background from $W \rightarrow \mu\nu_\mu$ process estimated from data

5.3 $W \rightarrow \tau + \nu$

In case of W decays to $\tau + \nu$, there are more ways to contribute to backgrounds.

If it is W + 1 jet, the τ decays to hadrons which form a jet, and the two neutrinos can cause a large amount of $\not{E}_T$. It adds to the background.

If it is W + 2 or more jets, the τ could decay to muon or electron as well as hadrons. In any case if it is not rejected by the previous cuts. It becomes our background.

We found nine $W \rightarrow \tau\nu$ candidates in our final data set. These were of hadronic decay mode, and with τ cluster $E_T > 20$ GeV.

The $\not{E}_T$ distribution from STIRLING $W \rightarrow \tau\nu_\tau$ events which pass the cuts is shown in Figure 5.6.

Backgrounds from $W \rightarrow \tau\nu_\tau$ events can be simulated by the same method used in $W \rightarrow \mu + \nu$ analysis. The only difference is to replace the electron energy deposition in the calorimeters with the proper energy deposition by a τ. Since the dominant contribution from $W \rightarrow \tau\nu_\tau$ is $W + 1$ jet where the τ decays to hadrons, the simulation was done assuming all τ's decayed into hadrons + ν_τ.

For this study a slightly different data set and slightly different electron cuts were used for practical reasons. The cuts are listed in Appendix D.

The background contribution from $W \rightarrow \tau + \nu$ is

$$N(W \rightarrow \tau + \nu) = \frac{n_\tau}{\epsilon_{c\tau}\epsilon_{ele}\epsilon_{eb}\epsilon_\tau} Br\epsilon_{trg},$$

where

$\epsilon_\tau = 0.44 \pm 0.07$ is the ratio of the number of events passed our cuts in which τ decays to hadrons with $P_T(\tau) > 20$ GeV and $|\eta| < 1.0$, to the number of total events passed our cuts from $W \rightarrow \tau + \nu$ process,

Br = 0.65 ± 0.01 is the branch ratio for τ decaying to hadrons,

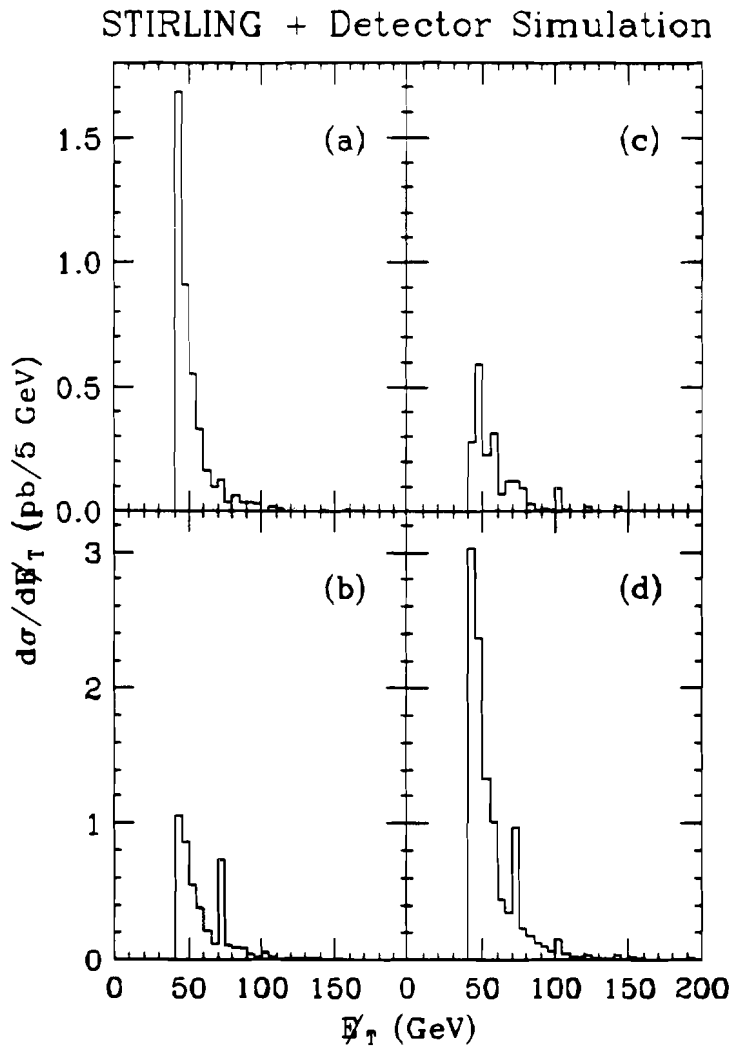

Figure 5.6: Background from Stirling Monte Carlo $W \to \tau\nu_\tau$ processes: (a) W + 1 jet, (b) W + 2 jets, (c) W + 3 jets and (d) sum of W + 1,2,3 jets

$\epsilon_{eb} = 0.92 \pm 0.02$ [65] is the efficiency for Track-Strip match and border energy cuts.

With $n_\tau = 15$ events passed cuts from this simulation, the background contribution from $W \to \tau - \nu$ is

$$N(W \to \tau + \nu) = 30.7.$$

Their $\not{E}_T$ distribution is shown in Figure 5.7.

5.4 $Z \to \nu\bar{\nu}$

A neutrino leaves no signals in the detector. So for Z + 2 or more jets event, it is very easy to enter into the background as long as it satisfies the kinematic cuts.

The $\not{E}_T$ distribution from STIRLING $Z \to \nu\bar{\nu}$ events which pass the cuts is shown in Figure 5.8.

For Z + jets events, their Z P_T distribution has the same shape as W + jets events (see Figure 5.9). So it is possible to simulate $Z \to \nu + \bar{\nu}$ events by removing the electron energy in $W \to e + \nu$ events. (The $W \to e + \nu$ data set was chosen rather than the $Z \to \nu\bar{\nu}$ data, since there are approximately 10 times more W events. This allows more certainty in prediction of the $\not{E}_T$ distribution.)

The expected background is

$$N(Z \to \nu + \bar{\nu}) = \frac{n_\nu}{\epsilon_{cr}\epsilon_{ele}\epsilon_{el}\epsilon_{M_t}\epsilon_v} R\epsilon_{trg},$$

where $R = \frac{\sigma(p\bar{p} \to Z \to \nu + \bar{\nu})}{\sigma(p\bar{p} \to W \to e + \nu)} = 0.59 \pm 0.03$ is derived from our own measurement [61].

Using the data discussed in $W \to \mu\nu$ case, we have

$$N(Z \to \nu + \bar{\nu}) = 32.7.$$

The $\not{E}_T$ distribution is shown in Figure 5.10.

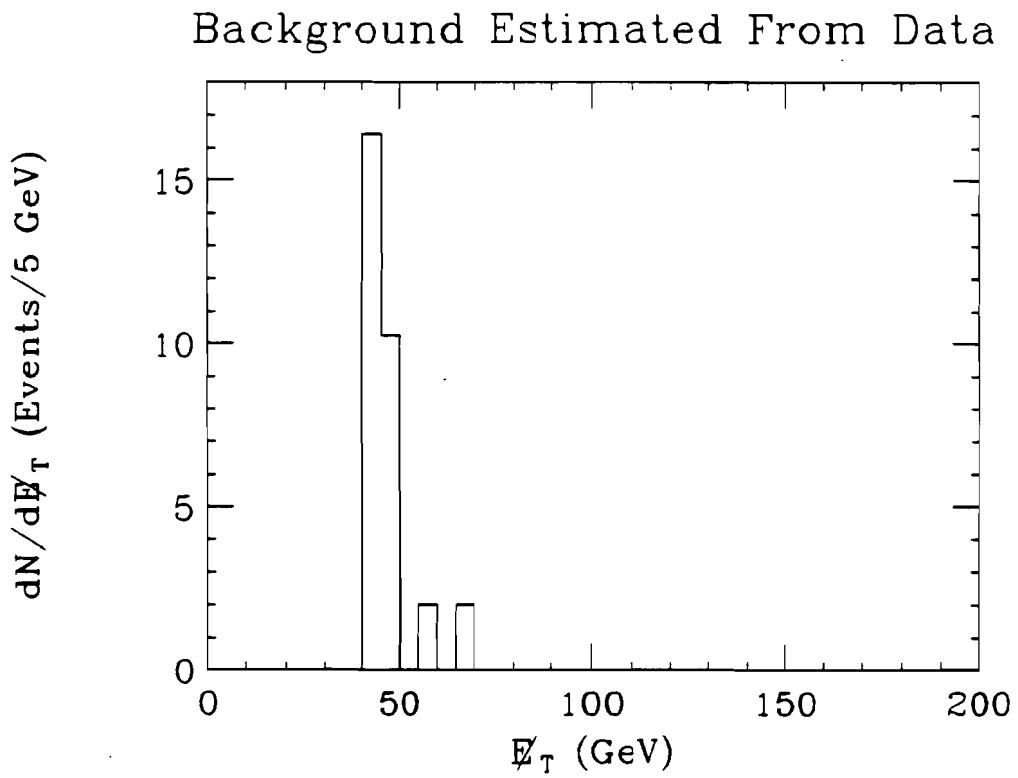

Figure 5.7: Background from $W \rightarrow \tau\nu_\tau$ process estimated from data

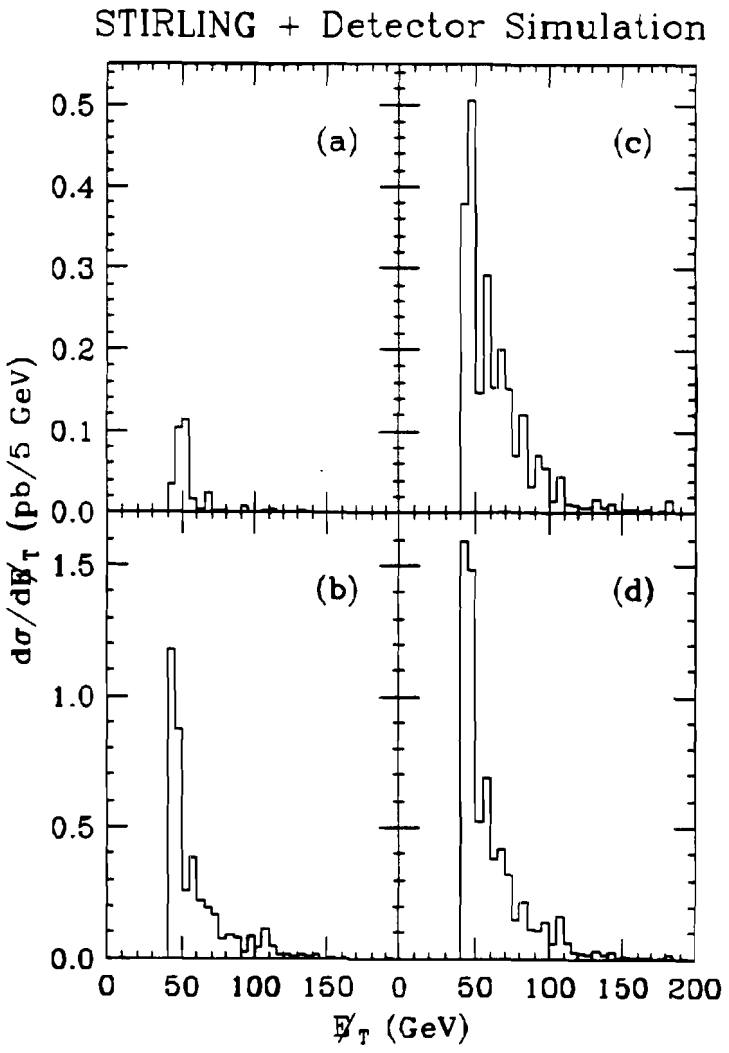

Figure 5.8: Background from Stirling Monte Carlo $Z \to \nu\bar{\nu}$ processes: (a) Z + 1 jet, (b) Z + 2 jets, (c) Z + 3 jets and (d) sum of Z + 1,2,3 jets

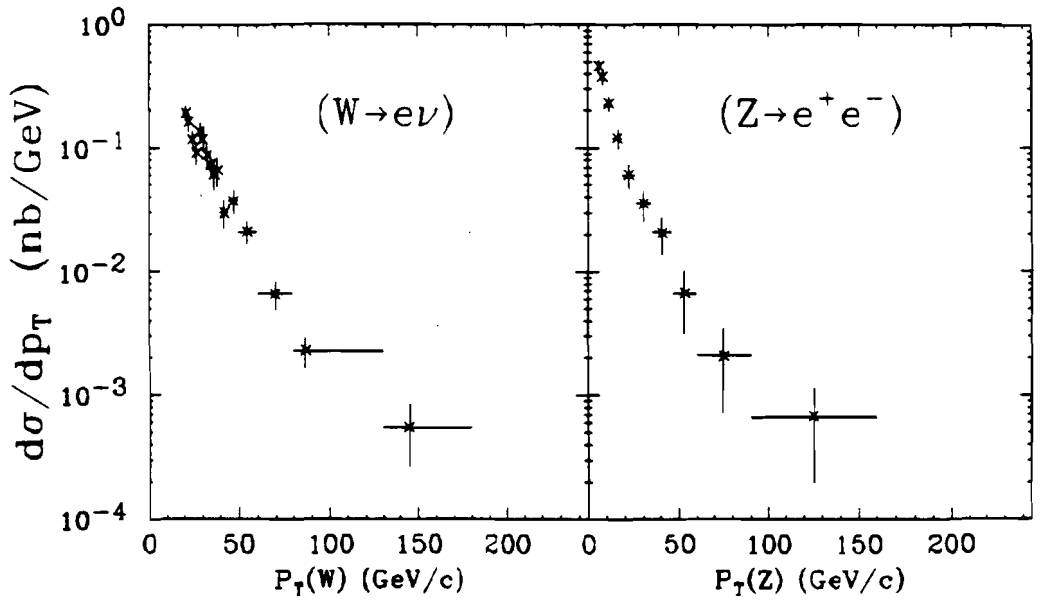

Figure 5.9: $W(Z)$ P_T distribution in $W(Z)$ + jets events. The W and Z distributions have been divided by the branching fraction for the observed decay mode.

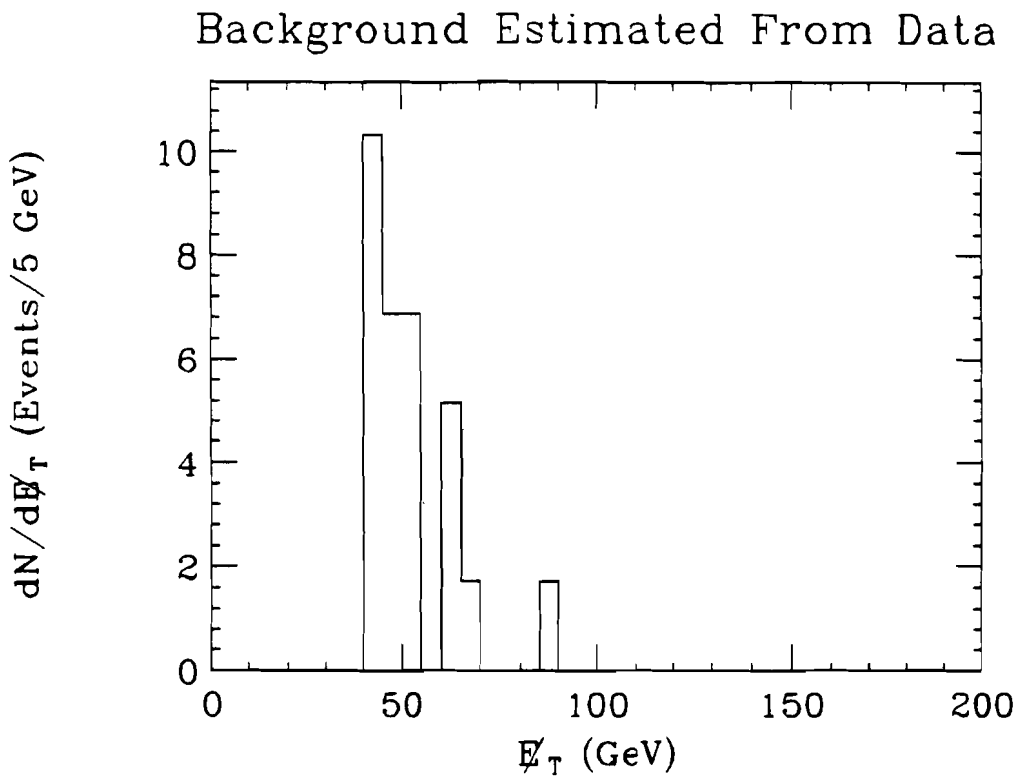

Figure 5.10: Background from $Z \rightarrow \nu\bar{\nu}$ process estimated from data

5.5 QCD Events

The major background from QCD processes comes from the heavy quarks, especially $b\bar{b}$. If the $b(\bar{b})$ decays to leptons the neutrino is usually very close to the $b(\bar{b})$ jet. Most of them could be rejected by our cuts, but those that survive contribute to the background.

Finally, if one of the jets in the standard QCD events is mismeasured, it also can add to the background. But in this case the $\not{E}_T$ direction should be the same as that jet direction so that our cut should reject it unless the jet energy is completely lost or very low.

It is difficult to estimate the background from QCD processes. Different properties of the final data sample were checked to look for anomalies. Figure 5.11 is a plot of the angle between $\not{E}_T$ and the third jet ($E_T > 15$ GeV) direction in ϕ. There are some excess events in the small angle region (the low edge cut is 30°). However Monte Carlo studies for both the possible signal events (SUSY) and the $W(Z)$ + jets background predict a flat distribution. Therefore we attributed the excess of events to either mismeasured QCD events or $b(\bar{b})$ quark decay. The estimated background from QCD processes is 4 ± 4 events. It is noticed that these events with the third jet close to the $\not{E}_T$ direction all have $\not{E}_T$ below 45 GeV. In other words they barely pass the 40 GeV threshold. This is just what one can expect from QCD events.

5.6 Summary

Two methods were used to determine backgrounds for the SUSY signal: a Monte Carlo calculation and estimates based on distributions observed in data.

As shown in previous sections, the background contributions from $W(Z)$ + jet(s) were estimated from STIRLING Monte Carlo program. The sum of these contributions determined in this way is shown in Figure 5.12.

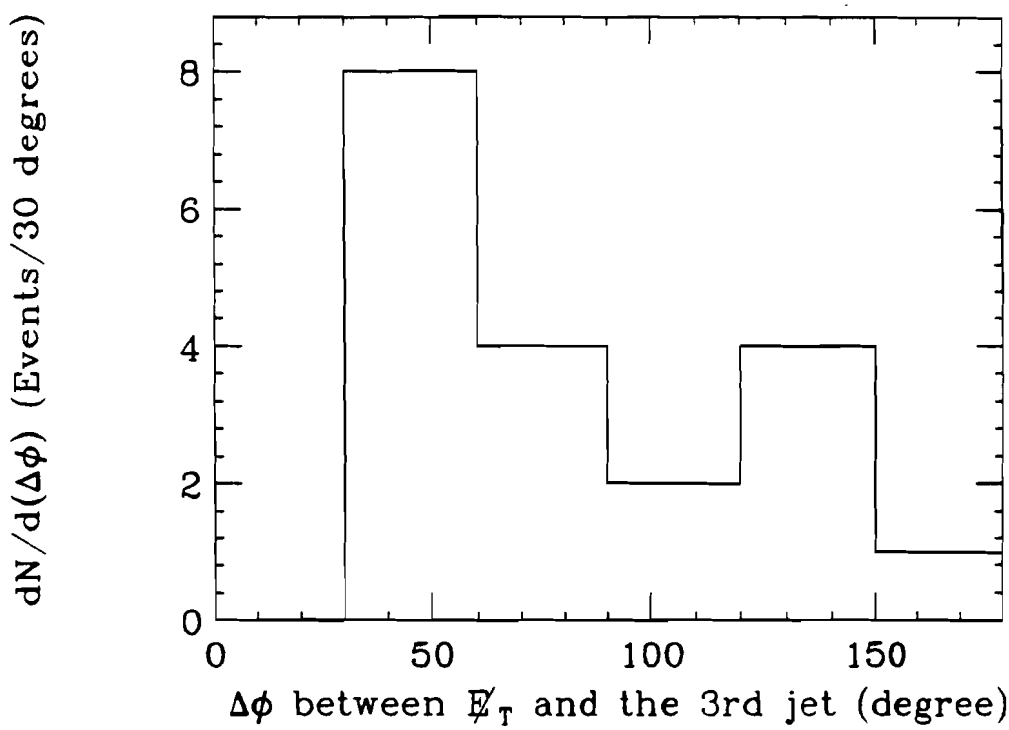

Figure 5.11: $\Delta\phi$ between $\not{E}_T$ and the third jet

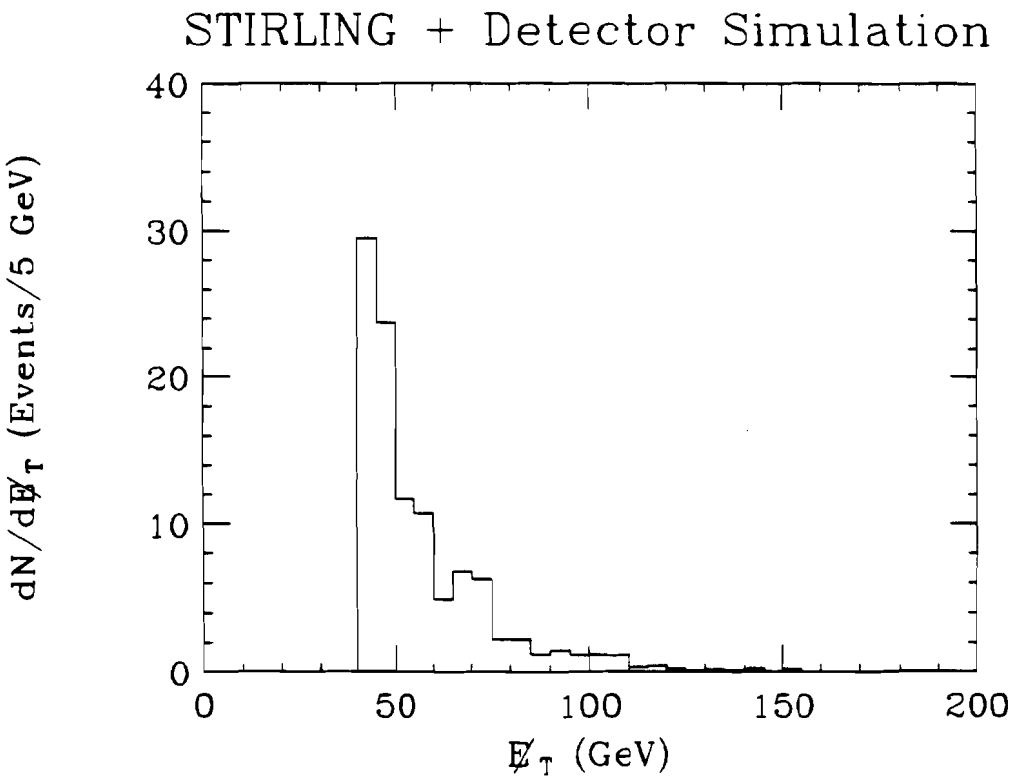

Figure 5.12: $\not{E}_T$ distribution for $W(Z)$ + jet(s) background from STIRLING

The estimation of background events from our own data shows that the background contributions are $88.6 \pm 14.5(\text{stat}) \pm 10.3(\text{sys})$ events from $W(Z)$ decay and 4 ± 4 events from QCD. The $\not{E}_T$ distribution from the $W(Z) - \text{jet(s)}$ events is shown in Figure 5.13.

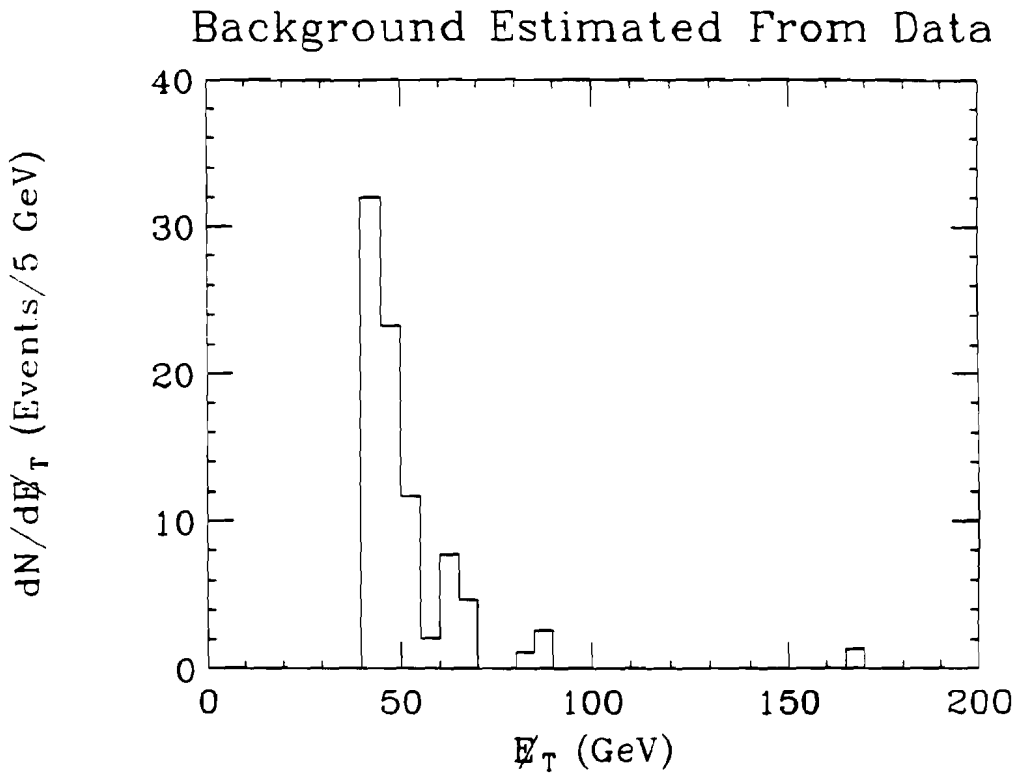

Figure 5.13: $\not{E}_T$ distribution for background estimated from CDF data sample

Chapter 6

Data Analysis: Monte Carlo Study of SUSY Signal

The ISAJET Monte Carlo program was used to generate the SUSY events and a CDF detector simulation program was used to simulate the calorimetry response for these events. Then the same cuts as described before were applied to these events. For different SUSY particle masses, the production cross sections and the cuts' efficiencies are different, because the $\not{E}_T$ distribution is dependent on SUSY particle masses. Figure 6.1 shows the $\not{E}_T$ distribution for some SUSY particle masses.

Systematic Uncertainty

The systematic uncertainty for our expected SUSY events comes from the following factors.

- The uncertainty of our integrated luminosity is 15%.
- The uncertainty of ISAJET Monte Carlo includes the choice of Q^2 and the limited number of events which were generated. The estimated uncertainty is about 15%.
- The choice of structure function could induce further uncertainty, but the EHLQ1, which was used in this analysis, has the lowest predicted cross sections. This ensures that, with respect to structure functions, the conclusions reached are conservative.

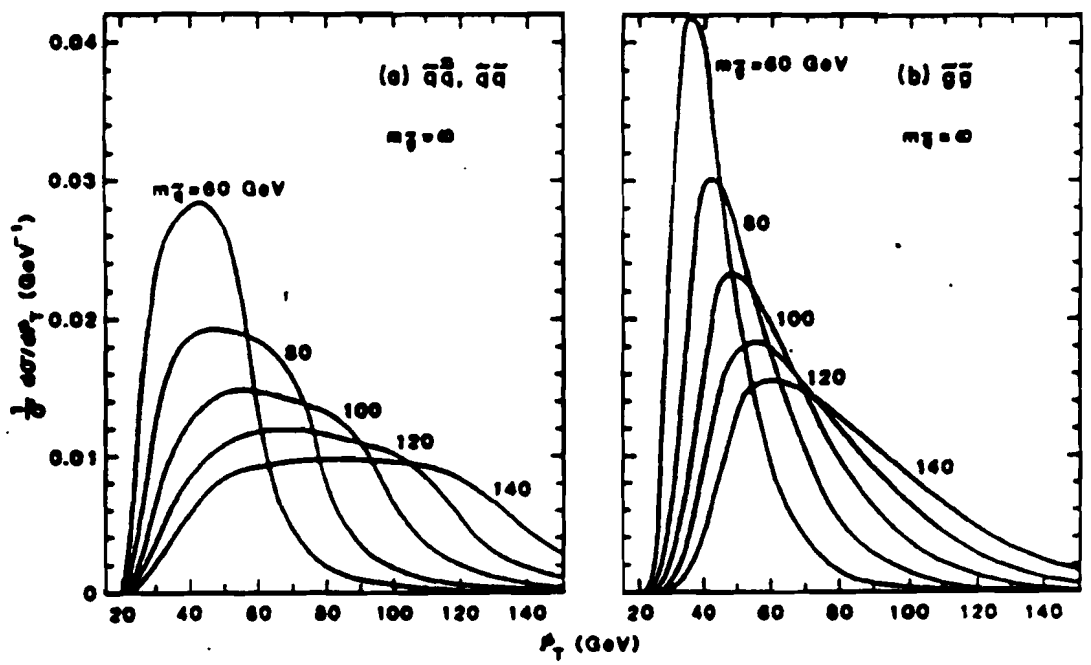

Figure 6.1: Distribution in missing P_T (adapted from Baer and Berger [21]) for two extreme cases of (a) $\tilde{q}\bar{\tilde{q}}$ and $\tilde{q}\tilde{q}$ production with $m_{\tilde{g}} = \infty$ and (b) $\tilde{g}\tilde{g}$ production with $m_{\tilde{q}} = \infty$. The area under the curved is normalized to unity; the results are insensitive to collider energy between 0.5 and 2 TeV.

- There is an uncertainty in the jet energy and the overall calorimeter energy scale. The energy scale in the detector simulation were changed by 10% to study this effect. The energy scale was also changed 5% in central region and 10% in the rest. In both case the expected SUSY events changed less than 1%.

- The Level 2 $\not{E}_T$ trigger efficiency is about $92.4 \pm 2.4\%$.

So that the total uncertainty is about 21%.

For the background, when the estimated number of events from our own data was used, there was no systematic uncertainty from luminosity, choices of Q^2 and structure function, jet energy and overall energy scale, etc. The only uncertainty comes from the cuts' efficiency and acceptance which were discussed in the last chapter. The uncertainty of the acceptance partly comes from Monte Carlo from which ϵ_e, ϵ_ν and ϵ_τ were derived. Because STIRLING only has W (Z) + 1,2,3 jets, the acceptances for 1 and 2 jets and for 1, 2 and 3 jets were compared to estimate the additional contribution of 4 or more jets. The acceptances for different choice of structure functions were also studied, as were the acceptances from the different Monte Carlo program — PAPAGENO, STIRLING and ISAJET. Their predicted acceptance were very similar, usually differing by less than 1%.

Chapter 7

Data Analysis: SUSY Particle Mass Limits

As discussed before there was no excess of events with large $\not{E}_T$ in the final data set. This can be used to derive limits on SUSY particle production.

From Figure 2.2, 2.3 and 2.4, one can see that when $\tilde{q}$ mass is lower than $\tilde{g}$ mass the events should have two jets with large $\not{E}_T$; if the $\tilde{g}$ mass is lower the events would have four jets. So the limits were studied in these two cases.

7.1 $M_{\tilde{q}} < M_{\tilde{g}}$

In this case one can look for events with $\not{E}_T$ greater than a certain threshold. For different $\tilde{q}$ mass, the $\not{E}_T$ distribution and the production cross section are different. As the $\tilde{q}$ mass increases, the production cross section decreases and the peak in $\not{E}_T$ distribution shifts to high $\not{E}_T$ region. So it is helpful to use a high $\not{E}_T$ threshold to get the limit. Table 7.1 shows the cross section and expected number of events with $\not{E}_T > 40$ GeV and $\not{E}_T > 100$ GeV for some squark and gluino mass combinations. The numbers of expected event in the table are normalized to corresponding to 4.3 pb^{-1} data.

The events with $\not{E}_T > 40$ GeV were used to exclude the region 70 GeV/c^2 < $M_{\tilde{q}} < 130$ GeV/c^2. The $\not{E}_T$ threshold was increased to 100 GeV to calculate the 90% confidence level (CL) limits. There was 3 events from the final data set and the estimated background from the data is 1.3±1.3 events. Using the method described in Appendix E, the 90% CL limit is 6.4 events assuming $\not{E}_T$ trigger efficiency is 92.4%.

$(m_{\tilde{g}}, m_{\tilde{q}})$	σ (pb)	# of events expected to pass the cuts	
		$\not{E}_T > 40$ GeV	$\not{E}_T > 100$ GeV
(230,230)	5.50	7.8	5.0
(225,225)	6.67	9.5	5.9
(250,215)	6.11	9.2	5.8
(250,210)	6.83	10.8	6.5
(250,205)	7.85	12.4	7.6
(300,200)	6.26	-	5.4
(300,190)	8.33	-	6.6
(300,180)	11.2	-	7.4
(300,170)	15.1	-	8.7
(300,160)	20.8	-	10.1
(350,190)	6.66	10.6	5.5
(350,180)	8.83	13.6	6.6
(350,170)	12.3	18.5	7.8
(400,175)	8.89	12.9	4.9
(400,170)	10.6	13.5	5.7
(400,165)	12.7	19.5	7.4
(400,160)	14.4	20.3	7.5
(400,155)	17.3	25.1	7.8
(400,150)	21.1	28.4	8.1
(400,145)	24.8	33.5	8.2
(400,140)	29.9	33.5	7.4
(300,150)	28.8	38.3	11.3
(400,150)	21.1	28.4	8.0
(500,150)	17.0	22.6	6.0
(600,150)	14.5	19.5	5.1
(700,150)	12.3	15.5	3.6
(800,150)	11.1	15.0	4.1
(900,150)	10.3	13.6	3.9
(1000,150)	9.72	13.3	3.3

Table 7.1: SUSY particle production cross sections and expected number of events passed cuts. with $\not{E}_T > 100$ GeV and $\not{E}_T > 40$ GeV. The statistic uncertainties are typically 5% and systematic uncertainty about 20%. "-" not studied.

$(m_{\tilde{g}}, m_{\tilde{q}})$	σ (pb)	# of events ($\geq$ 2 jets)	# of events ($\geq$ 4 jets)
(190,190)	24.9	31.3	3.4
(170,170)	56.3	67.8	7.8
(180,190)	30.3	-	5.9
(180,200)	25.4	-	4.2
(170,200)	31.4	-	6.0
(170,220)	24.5	-	4.4
(165,220)	27.8	-	4.9
(165,250)	20.5	12.1	4.8
(155,250)	29.7	16.8	5.2
(155,300)	32.3	20.2	5.0
(155,400)	24.5	15.1	2.7
(150,400)	32.2	21.5	5.4
(150,500)	34.0	21.6	4.8
(145,500)	43.4	-	6.0
(140,500)	55.3	-	6.3

Table 7.2: SUSY particle production cross sections and expected number of events passed cuts with $\not{E}_T > 40$ GeV and at least 4 jets $E_T > 15$ GeV. The statistic uncertainties are typically 5% and systematic uncertainty about 20%."-" not studied.

7.2 $M_{\tilde{q}} > M_{\tilde{g}}$

The limits were decided by the events with 4 or more jets $E_T > 15$ GeV in this case. There were 2 events of this kind on the final data set, and the estimated background is 1.3±1.3 events. This leads to a 90% CL limit of 5.0 events with $\not{E}_T$ efficiency 92.4%. Table 7.2 shows some expected number of events for 4.3 pb^{-1} from the different $\tilde{g}$ and $\tilde{q}$ mass combinations.

The 90% confidence level (CL) limit is shown in Figure 7.1.

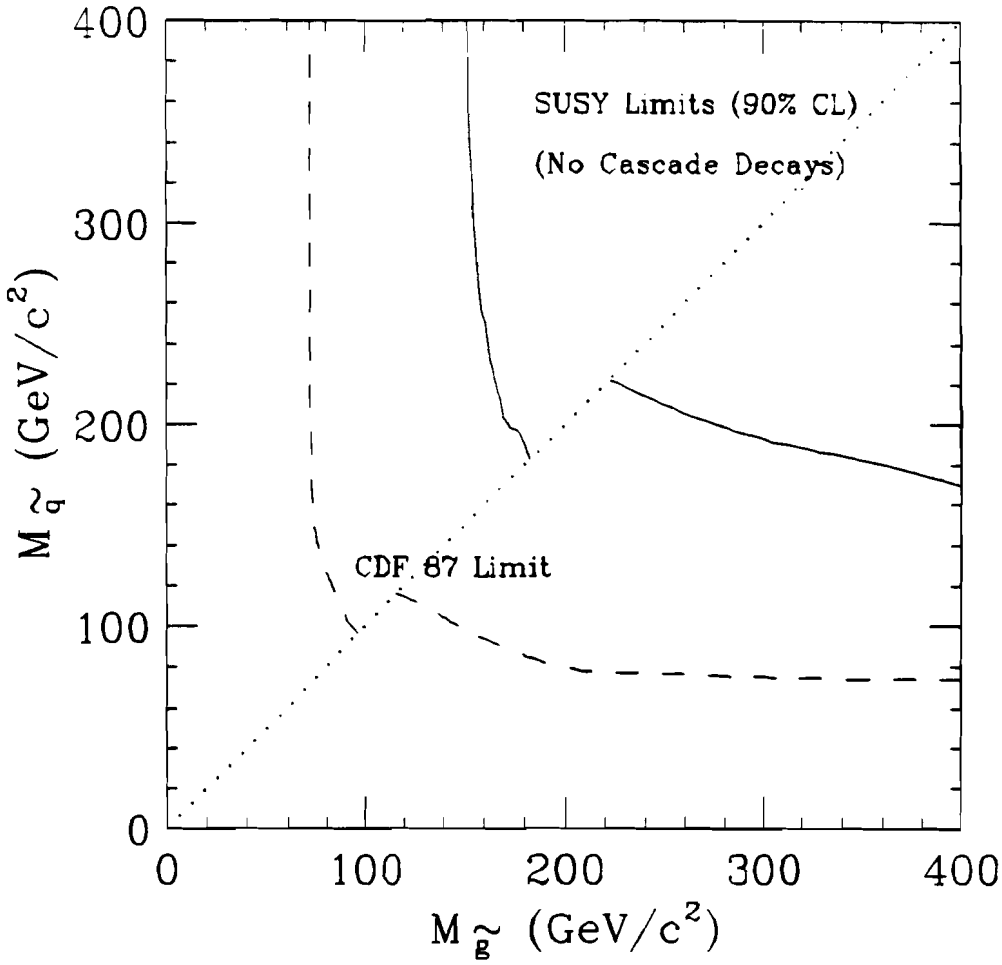

Figure 7.1: $\tilde{q}$ and $\tilde{g}$ mass limits at 90% confidence level. The previous limits are also shown in the plot.

Chapter 8

Summary

In conclusion, the study of a $\not\!\!E_T$ data set corresponding to 4.3 pb^{-1} data from $p\bar{p}$ collision at $\sqrt{s} = 1.8$ TeV shows that the data are consistent with the Standard Model prediction. There were no excess events which suggests a SUSY particle's existence.

Based on the theoretical assumptions discussed in earlier chapters, The 90% CL limits on SUSY particle's masses were reached which are shown in Figure 7.1.

The results presented in this thesis would change for different photino mass and different decay modes. The production for unequal left-handed and right-handed squark masses was discussed by H. Baer and X. Tata [66]. If some gauginos' masses are lighter than squark's mass, squarks could decay to the gaugino and subsequently decay to the LSP. Such cascade decay mode has been discussed by some theorists [67,68]. The event signature in this case would be m leptons $-$ n jets $-$ $\not\!\!E_T$, but $\not\!\!E_T$ would be degraded comparing with the $\not\!\!E_T$ in decay modes used in this thesis.

The direct search for gauginos was also suggested by theorists [69]. These studies could be carried out in the near future. The results would tell us whether there are any such SUSY particles with masses up to 200 GeV, and perhaps give us some hints if there are any new physics processes unexpected in the Standard Model.

Appendix A
The Colliders

The traditional method in particle physics experiment is to accelerate particles and let them collide with a stationary target — so-called "fixed target experiment". For many purposes, this works well, but the useful energy in such experiment is low. The center-of-mass (c.m.) energy when two relativistic particles collide is given by the following formula

$$E_{cms} = \sqrt{(E_1 - E_2)^2 - (P_{x1} + P_{x2})^2 - (P_{y1} - P_{y2})^2 - (P_{z1} - P_{z2})^2} \qquad (A.1)$$

where $(E_1, P_{x1}, P_{y1}, P_{z1})$ and $(E_2, P_{x2}, P_{y2}, P_{z2})$ are the four-momenta of the two particles. For fixed target experiment, one particle is moving $(E, 0, 0, p)$ and the other is at rest $(M, 0, 0, 0)$, the center-of-mass energy is

$$E_{cms} = \sqrt{(E + M)^2 - p^2} \qquad (A.2)$$

The moving particle has mass $m = \sqrt{E^2 - p^2}$, and $m, M \ll E$, so

$$E_{cms} = \sqrt{2EM + M^2 + m^2} \approx \sqrt{2EM} \qquad (A.3)$$

The c.m. energy grows as the square-root of the beam energy. Thus, the 800 GeV energy of the Fermilab Tevatron in fixed-target operation yields $E_{cms} \approx 40$ GeV in the proton-nucleon c.m. system.

In order to use the beam energy more efficiently and to achieve high energy, it is necessary to have a "head-on" collision of two moving particles. Assuming their four momenta are $(E_1, 0, 0, p_1)$ and $(E_2, 0, 0, -p_2)$,

$$E_{cms} = \sqrt{(E_1 + E_2)^2 - (p_1 - p_2)^2} \qquad (A.4)$$

If $p_1 = p_2$,

$$E_{cms} = E_1 - E_2 \tag{A.5}$$

In this way, the scaling is linear and a high center-of-mass energy can be reached. In collider operation at Fermilab, $E_1 = E_2 = 900$ GeV and $E_{cms} = 1800$ GeV.

At the Tevatron, the $p\bar{p}$ center of mass energy is 1800 GeV, and parton-parton c.m. energies of order 400 GeV are typical. This is significantly higher than the electroweak scale of 100 GeV, and it is possible to study phenomenon predicted by theory and to search for new discoveries either by their direct appearance or by departure from the standard model prediction.

Appendix B

Cuts Used in Spin Cycle

The events which passed one of the filter algorithms — METFLT, DFEXPR and TOP_EXPRESS, were written to the SFL output tapes in the Spin Cycle. The cuts in these filter algorithm are listed below.

METFLT ("$\not{E}_T$ Filter"):

Events pass all following requirements.

- $\not{E}_T > 20$ GeV
- $\sigma_{\not{E}_T} > 2.4$
- The leading jet cluster must be in the good detector region ($|\eta| < 3.5$), and have at least 5% of its energy deposited in the electromagnetic calorimeters.
- If the event had a jet cluster with $E_T > 5$ GeV within 30° opposite to the leading jet cluster in ϕ direction, the event was removed from the data set.

DFEXPR ("Damn Fast Express", leptons and photons):

Events pass one of the following requirements.

- Single Photon: $E_T > 150.0$ GeV
- Di-Photon: $E_T > 20.0$ GeV
- Single Electron: $E_T > 20.0$ GeV, $P_T > 15.0$ GeV
- Di-Electron: $E_T > 8.0$ GeV, $P_T > 8.0$ GeV
- Single Muon: $P_T > 20.0$ GeV

- Di-Muon: $P_T > 5.0$ GeV
- Single Central Jet: $E_T > 100.0$ GeV
- Di-Central-Jet: $E_T > 80.0$ GeV
- Muon-Electron: Muon $P_T > 5.0$ GeV, Electron $E_T > 5.0$ GeV
- Muon-Gamma: Muon $P_T > 10.0$ GeV, Photon $E_T > 10.0$ GeV
- E-Gamma: Electron $E_T > 10.0$ GeV, Photon $E_T > 10.0$ GeV
- Muon − Cental Jet: Jet $E_T > 20.0$ GeV, Muon $P_T > 15.0$ GeV
- Electron + Central Jet: Jet $E_T > 20.0$ GeV, Electron $E_T > 15.0$ GeV
- Photon+ $\not{E}_T$: Photon $E_T > 20.0$ GeV, $\not{E}_T > 20.0$ GeV
- Sum E_T : $\sum E_T > 180.0$ GeV
- Single Isolated track: $P_T > 30.0$ GeV
- Isolated Track + $\not{E}_T$: Track $P_T > 20.0$ GeV, $\not{E}_T > 20.0$ GeV
- Minimum Ionized Isolated Track: $P_T > 20.0$ GeV, $E_{T\ max}$ in wedge < 4.0 GeV

TOP_EXPRESS:

Events pass one of the following requirements.

- Jet Cuts: $E_{T\ jet} > 8.0$ GeV, $|\eta_{jet}| < 2.0$ and no jets with electron,
- Electron Cuts: Electron is in central calorimeter, $E_T > 12.0$ GeV, $E_{had}/E_{EM} < 0.1$, $P_T > 10$ GeV/c, LSHR < 0.3 and $\chi^2_{strip} < 10.0$,
- Muon Cuts: CFT bin > 4, number of jets > 2 with $E_T > 10.0$ GeV, and minimum ϕ between muon and jet is 7.5°.

Appendix C

$W \rightarrow e + \nu$ Selection 1

The following cuts were applied an inclusive electron data sample to select the $W \rightarrow e + \nu$ events.

- $P_T(ele) > 15$ GeV and $|\eta| < 1.0$
- $|Q_{ELES}| = 1$
- $\not{E}_T > 15$ GeV
- $E_T/P_T < 1.5$ if $E_T < 50$ GeV
- $E_{had}/E_{EM} < 0.055 + 0.00045 E_T(\mathrm{GeV})$
- CES $\chi^2_{strip} < 10$ and $\chi^2_{wire} < 10$, if $E_T < 50$ GeV
- LSHR < 0.2
- 40 GeV $< M_T <$ 100 GeV

P_T is the electron's transverse momentum measured from CTC. $E_T = E \sin\theta$, where E is the electron energy measured from calorimeter. Q_{ELES} is the electron charge determined by CTC tracking information. E_{had} and E_{EM} are the energies deposited in the hadron and electromagnetic calorimeter separately. The electron shower profiles in central strip and wire chambers were fit with the test beam measurements, χ^2_{strip} and χ^2_{wire} are the fitting χ^2 for them. LSHR is a lateral shower sharing variable, it is defined as

$$\mathrm{LSHR} = 0.14 \sum_i \frac{M_i - P_i}{\sqrt{0.14^2 E_{cl} + dP_i^2}},$$

where energy and momenta are in GeV, the sum is over towers adjacent to the seed tower in the cluster and

- M_i is the measured energy fraction of the adjacent tower energy to the sum of it and the seed tower energy,
- P_i is the energy fraction calculated using the impact point in Z, the event vertex and the shower profile fit obtained from test beam data,
- E_{cl} is the cluster electromagnetic energy,
- dP_i is the uncertainty in P_i associated with a 1 *cm* variation in impact point at the strip chamber.

The transverse mass of electron and $\not{E}_T$ is defined as $M_T = 2E_T\not{E}_T\,(1 - \cos\phi)$, where E_T is the transverse energy of electron and ϕ is the azimuthal angle between the electron and $\not{E}_T$ vectors.

Appendix D

$W \rightarrow e + \nu$ Selection 2

The following cuts were applied a W and Z data sample to select the $W \rightarrow e + \nu$ events.

- $P_T(ele) > 20$ GeV and $\eta < 1.0$
- $\not{E}_T > 20$ GeV
- $E_T/P_T < 1.5$ if $E_T < 50$ GeV
- $E_{had}/E_{EM} < 0.055 - 0.00045 E_T(\mathrm{GeV})$
- CES $\chi^2_{strip} < 10$ and $\chi^2_{wire} < 10$, if $E_T < 50$ GeV
- LSHR < 0.2
- the Track-Strip match (1.5cm in η-ϕ and 3.0cm in Z)
- border tower energy less than 2 GeV.

P_T is the electron's transverse momentum measured from CTC. $E_T = E \sin\theta$. where E is the electron energy measured from calorimeter. E_{had} and E_{EM} are the energies deposited in the hadron and electromagnetic calorimeter separately. The electron shower profiles in central strip and wire chambers were fit with the test beam measurements, χ^2_{strip} and χ^2_{wire} are the fitting χ^2 for them. LSHR is a lateral shower sharing variable, it is defined as

$$\mathrm{LSHR} = 0.14 \sum_i \frac{M_i - P_i}{\sqrt{0.14^2 E_{cl} + dP_i^2}},$$

where energy and momenta are in GeV, the sum is over towers adjacent to the seed tower in the cluster and

- M_i is the measured energy fraction of the adjacent tower energy to the sum of it and the seed tower energy,
- P_i is the energy fraction calculated using the impact point in Z, the event vertex and the shower profile fit obtained from test beam data.
- E_{cl} is the cluster electromagnetic energy,
- dP_i is the uncertainty in P_i associated with a 1 cm variation in impact point at the strip chamber.

Appendix E

Method Used in Determination of the Upper Limit

The method to determine the upper limit from an experiment has been discussed in many papers. One of the most recent articles is from G. Zech [70].

If the probability, p, of a particular kind of events occurred in our measurement, is very small, and we repeat the measurement N times, then the probability of this kind events happened would follow Possion distribution

$$P(n;\mu) = \frac{e^{-\mu}\mu^n}{n!}.$$

Where $\mu = pN$, n is the number of times the special kind of events happened.

If we expect μ events in our experiment, and we only saw n_0 events, then the probability of observing more than n_0 events if we repeat our experiment would be

$$\begin{aligned} CL &= \sum_{i=n_0+1}^{\infty} P(i;\mu) \\ &= 1 - \sum_{i=0}^{n_0} P(i;\mu). \end{aligned}$$

So that if CL is our desired confidence level, the upper limit for allowed expected events would be μ.

If the number of expected events has a relative uncertainty η, and it follows Gaussian distribution

$$G(\mu;\mu_0,\sigma) = \frac{1}{\sigma\sqrt{2\pi}} e^{-\frac{(\mu-\mu_0)^2}{2\sigma^2}}$$

where μ_0 is the number of expected events. $\sigma = \eta\mu_0$. The probability of observing n events would be

$$f(n;\mu_0,\sigma) = \frac{1}{k}\int_0^\infty P(n;\mu)G(\mu;\mu_0,\sigma)d\mu.$$

It has a normalization factor $k = \int_0^\infty G(\mu;\mu_0,\sigma)d\mu$. The above formula can be calculated as following

$$\begin{aligned}
f(n;\mu_0,\sigma) &= \frac{1}{k}\int_0^\infty \frac{e^{-\mu}\mu^n}{n!}\frac{1}{\sigma\sqrt{2\pi}}e^{-\frac{(\mu-\mu_0)^2}{2\sigma^2}}d\mu \\
&= \frac{1}{k\sigma\sqrt{2\pi}n!}\int_0^\infty \mu^n e^{-\frac{(\mu-\mu_0)^2}{2\sigma^2}-\mu}d\mu \\
&= \frac{1}{k\sigma\sqrt{2\pi}n!}\int_0^\infty \mu^n e^{-\frac{(\mu-(\mu_0-\sigma^2))^2+2\mu_0\sigma^2-\sigma^4}{2\sigma^2}}d\mu
\end{aligned}$$

If $\mu_0 \geq \sigma^2$, then

$$f(n;\mu_0,\sigma) = \frac{e^{-(\mu_0-\frac{\sigma^2}{2})}}{k\sigma\sqrt{2\pi}n!}\left(\int_{\mu_0-\sigma^2}^\infty \mu^n e^{-\frac{(\mu-(\mu_0-\sigma^2))^2}{2\sigma^2}}d\mu + \int_0^{\mu_0-\sigma^2}\mu^n e^{-\frac{(\mu-(\mu_0-\sigma^2))^2}{2\sigma^2}}d\mu\right)$$

With substitution $z = (\frac{\mu-(\mu_0-\sigma^2)}{\sigma})^2$,

$$\begin{aligned}
f(n;\mu_0,\sigma) &= \frac{e^{-(\mu_0-\frac{\sigma^2}{2})}}{k\sigma\sqrt{2\pi}n!}\left(\int_0^\infty(\mu_0-\sigma^2+\sigma\sqrt{z})^n\frac{\sigma}{2\sqrt{z}}e^{-\frac{z}{2}}dz\right. \\
&\quad \left.+\int_{(\frac{\mu_0-\sigma^2}{\sigma})^2}^0(\mu_0-\sigma^2-\sigma\sqrt{z})^n(-\frac{\sigma}{2\sqrt{z}})e^{-\frac{z}{2}}dz\right) \\
&= \frac{e^{-(\mu_0-\frac{\sigma^2}{2})}}{2k\sqrt{2\pi}n!}\left(\int_0^\infty(\mu_0-\sigma^2+\sigma\sqrt{z})^n z^{-\frac{1}{2}}e^{-\frac{z}{2}}dz\right. \\
&\quad \left.+\int_0^{(\frac{\mu_0-\sigma^2}{\sigma})^2}(\mu_0-\sigma^2-\sigma\sqrt{z})^n z^{-\frac{1}{2}}e^{-\frac{z}{2}}dz\right. \\
&= \frac{e^{-(\mu_0-\frac{\sigma^2}{2})}}{2k\sqrt{2\pi}n!}\left(\int_0^\infty\left(\sum_{m=0}^n\frac{n!}{m!(n-m)!}(\mu_0-\sigma^2)^{n-m}\sigma^m z^{\frac{m}{2}}\right)z^{-\frac{1}{2}}e^{-\frac{z}{2}}dz\right. \\
&\quad \left.+\int_0^{(\frac{\mu_0-\sigma^2}{\sigma})^2}\left(\sum_{m=0}^n\frac{n!(-1)^m}{m!(n-m)!}(\mu_0-\sigma^2)^{n-m}\sigma^m z^{\frac{m}{2}}z^{-\frac{1}{2}}e^{-\frac{z}{2}}dz\right)\right. \\
&= \frac{e^{-(\mu_0-\frac{\sigma^2}{2})}}{2k\sqrt{2\pi}}\left(\sum_{m=0}^n\frac{(\mu_0-\sigma^2)^{n-m}\sigma^m}{m!(n-m)!}\left(\int_0^\infty z^{\frac{m-1}{2}}e^{-\frac{z}{2}}dz\right.\right. \\
&\quad \left.\left.+(-1)^m\int_0^{(\frac{\mu_0-\sigma^2}{\sigma})^2}z^{\frac{m-1}{2}}e^{-\frac{z}{2}}dz\right)\right)
\end{aligned}$$

Recall the χ^2 distribution $p_{\chi^2}(z;n) = \frac{1}{2^{\frac{n}{2}}\Gamma(\frac{n}{2})} z^{\frac{n}{2}-1} e^{-\frac{z}{2}}$, we have

$$\begin{aligned} f(n;\mu_0,\sigma) &= \frac{e^{-(\mu_0-\frac{\sigma^2}{2})}}{2k\sqrt{2\pi}}\Big(\sum_{m=0}^{n}\frac{(\mu_0-\sigma^2)^{n-m}\sigma^m}{m!(n-m)!}2^{\frac{m+1}{2}}\Gamma(\frac{m-1}{2})\Big(\int_0^\infty p_{\chi^2}(z;n)dz \\ &\quad -(-1)^m\int_0^{(\frac{\mu_0-\sigma^2}{\sigma})^2} p_{\chi^2}(z;n)dz\Big)\Big) \\ &= \frac{e^{-(\mu_0-\frac{\sigma^2}{2})}}{2k\sqrt{2\pi}}\Big(\sum_{m=0}^{n}\frac{(\mu_0-\sigma^2)^{n-m}\sigma^m}{m!(n-m)!}2^{\frac{m+1}{2}}\Gamma(\frac{m-1}{2})\Big(1- \\ &\quad (-1)^m\int_0^{(\frac{\mu_0-\sigma^2}{\sigma})^2} p_{\chi^2}(z;n)dz\Big)\Big) \end{aligned}$$

If $\mu_0 < \sigma^2$, with the same procedure it is easy to get

$$f(n;\mu_0,\sigma) = \frac{e^{-(\mu_0-\frac{\sigma^2}{2})}}{2k\sqrt{2\pi}}\sum_{m=0}^{n}\frac{(\mu_0-\sigma^2)^{n-m}\sigma^m}{m!(n-m)!}2^{\frac{m+1}{2}}\Gamma(\frac{m-1}{2})\int_{(\frac{\mu_0-\sigma^2}{\sigma})^2}^{\infty} p_{\chi^2}(z;n)dz$$

Then we can use the same method to calculate CL as before.

$$CL = 1 - \sum_{i=0}^{n_0} f(i;\mu_0,\sigma).$$

If the experiment also has background, the expected number of background events is μ_b, the confidence level for an upper limit μ_0 is

$$CL = 1 - e^{-(\mu_b+\mu_0)}\sum_{n=0}^{n_0}\frac{(\mu_b-\mu_0)^n}{n!}/e^{-\mu_b}\sum_{n=0}^{n_0}\frac{\mu_b^n}{n!}$$

assuming there is no uncertainty.

If the expect background and signal also have uncertainty, assuming an uncertainty of background $\sigma_b = \eta_b\mu_b$. Then the probability to observe n events would be

$$P(n) = \sum_{n_1+n_2=n} f(n_1;\mu_0,\sigma)f(n_2;\mu_b,\sigma_b)/\sum_{i=0}^{n_0} f(i;\mu_b,\sigma_b).$$

And we still have

$$CL = 1 - \sum_{i=0}^{n_0} P(i).$$

References

[1] Sheldon L. Glashow. Partial-symmetries of Weak Interactions. *Nuclear Physics*, 22:579, 1961.

[2] Steven Weinberg. A Model of Leptons. *Physical Review Letters*, 19(21):1264, 1967.

[3] A. Salam. *Elementary Particle Theory: Relativistic Groups and Analyticity (Nobel Symposium No. 8)*. Almqvist and Wiksell, Stockholm, 1968.

[4] H. Fritzsch, W. A. Bardeen and M. Gell-Mann. *Scale and Conformal Symmetry in Hadron Physics*. Wiley, New York, 1973.

[5] David J. Gross and Frank Wilczek. Asymptotically Free Gauge Theories. i. *Physical Review D*, 8(10):3633, 1973.

[6] Steven Weinberg. Non-abelian Gauge Theories of the Strong Interactions. *Physical Review Letters*, 31(7):494, 1973.

[7] J. Illopoulos, S. L. Glashow and L. Maiani. Weak Interactions with Lepton-hadron Symmetry. *Physical Review D*, 2(7):1285, 1970.

[8] G. P. Yeh, Les Rencontres de Physique de la Valle d'Aoste, M. Greco Editor, Editions Frontieres, Gif-sur Yvette 1990.

[9] G. S. Abrams *et al.* Measurements of Z-boson Resonance Parameters in e^+e^- Annihilations. *Physical Review Letters*, 63(20):2173, 1989.

[10] ALEPH Collaboration. Determination of the Number of Light Neutrino Species. *Physics Letters B*, 231(4):519, 1989.

[11] DELPHI Collaboration. Measurements of the Mass and Width of the Z^0-particle from Multihadronic Final States Produced in e^+e^- Annihilations. *Physics Letters B*, 231(4):539, 1989.

[12] L3 Collaboration. A Determination of the Properties of the Neutral Intermediate Vector Boson Z^0. *Physics Letters B*, 231(4):509, 1989.

[13] OPEL Collaboration. Measurements of the Z^0 Mass and Width with the OPEL Detector at LEP. *Physics Letters B*, 231(4):530, 1989.

[14] ALEPH Collaboration. Search for Neutral Higgs Boson from Z^0 Decay in the Higgs Mass Range between 11 and 24 GeV. *Physics Letters B*, 241(1):141, 1990.

[15] J. Wess and B Zumino. Supergauge Transformations in Four Dimensions. *Nuclear Physics B*, 70:39, 1974.

[16] Vernon D. Barger and Roger J. N. Phillips. *Collider Physics*. Addison-Wesley Publishing Company, Inc., 1987.

[17] H. J. W. Muller-Kirsten and A. Wiedemann. *Supersymmetry*. World Scientific, 1987.

[18] Rabindra N. Mohapatra. *Unification and Supersymmetry*. Springer-Verlag, 1986.

[19] P. West. *Introduction to Supersymmetry and Supergravity*. World Scientific, 1986.

[20] E. Eichten, Sally Dawson and C. Quigg. Search for Supersymmetric Particles in Hadron-hadron Collisions. *Physical Review D*, 31(7):1581, 1985.

[21] H. Baer and E. L. Berger. Prospects for Supersymmetry at the Fermilab Collider. *Physical Review D*, 34(5):1361, 1986.

[22] P. R. Harrison and C. H. Llywellyn Smith. Hadroproduction of Supersymmetrice Particles. *Nuclear Physics B*, 213:223, 1983.

[23] AMY Collaboration. A Search for SUSY Particles in e^+e^- Annihilations at $\sqrt{s} = 50 - 60.8$ GeV. *Physics Letters B*, 234(4):534, 1990.

[24] TOPAZ Collaboration. Search for SUSY Particles in e^+e^- Annihilation at TRISTAN. *Physics Letters B*, 218(1):105, 1989.

[25] VENUS Collaboration. Search for SUSY Partners of Charged Letpons in e^+e^- Collisions with $\sqrt{s}$ up to 60.8 GeV. *Physics Letters B*, 234(1,2):202, 1990.

[26] L3 Collaboration. Mass Limits for Scalar Muons, Scalar Electrons, and Winos from e^+e^- Collsions near $\sqrt{s} = 91$ GeV. *Physics Letters B*, 233(3,4):530, 1989.

[27] OPEL Collaboration. A Search for Acoplanar Pairs of Leptons or Jets in Z^0 Decays. Mass Limits on Supersymmetric Particles. *Physics Letters B*, 240(1,2):261, 1990.

[28] UA1 Collaboration. Events with Large Missing Transverse Energy at the CERN Collider: iii. Mass Limits on Supersymmtric Particles. *Physics Letters B*, 198(2):261, 1987.

[29] F. Abe *et al.* Limits on the Masses of Supersymmetric Particles from 1.8-TeV $p\bar{p}$ Collisions. *Physical Review Letters*, 62(16):1825, 1989.

[30] UA2 Collaboration. A Search for Squark and Gluino Production at the CERN $p\bar{p}$ Collider. *Physics Letters B*, 235(3,4):363, 1990.

[31] UA2 Collaboration. Search for Scalar Electrons and Winos at the CERN $p\bar{p}$ Collider. *Physics Letters B*, 238(2,3,4):442, 1990.

[32] D. Ayres *et al.* Design Report for the Fermilab Collider Detector Facility (CDF). August 1981. Fermilab: Design Report.

[33] F. Abe *et al.* The CDF Detector: An Overview. *Nuclear Instruments and Methods in Physics Research*, A271:387, 1988.

[34] F. Snider *et al.* The CDF Vertex Time Projection Chamber System. *Nuclear Instruments and Methods in Physics Research*, A268:75, 1988.

[35] F. Bedeschi *et al.* Design and Construction of the CDF Central Tracking Chamber. *Nuclear Instruments and Methods in Physics Research*, A268:50, 1988.

[36] S. Bhadra *et al.* The Design and Construction of the CDF Central Drift Tube Array. *Nuclear Instruments and Methods in Physics Research*, A268:92, 1988.

[37] M. Atac *et al.* Radial Wire Drift Chambers for CDF Forward TRACKing. *Nuclear Instruments and Methods in Physics Research*, A269:40, 1988.

[38] S. Bhadra *et al.* A Computer-controlled Wire Tension Measurement System Used in the Fabrication of the CDF Central Drift Tube Array. *Nuclear Instruments and Methods in Physics Research*, A269:33, 1988.

[39] L. Balka *et al.* The CDF Central Electromagnetic Calorimeter. *Nuclear Instruments and Methods in Physics Research*, A267:272, 1988.

[40] S. Bertolucci *et al.* The CDF Central and Endwall Hadron Calorimeter. *Nuclear Instruments and Methods in Physics Research*, A267:301, 1988.

[41] Y. Fukui *et al.* CDF End Plug Electromagnetic Calorimeter Using Conductive Plastic Proportional Tubes. *Nuclear Instruments and Methods in Physics Research*, A267:280, 1988.

[42] G. Brandenburg *et al.* An Electromagnetic Calorimeter for the Small Angle Regions of the Collider Detector at Fermilab. *Nuclear Instruments and Methods in Physics Research*, A267:257, 1988.

[43] S. Cihangir *et al.* The CDF Forward/backward Hadron Calorimeter. *Nuclear Instruments and Methods in Physics Research*, A267:249, 1988.

[44] S. R. Hahn *et al.* Calibration Systems for the CDF Central Electromagnetic Calorimeter. *Nuclear Instruments and Methods in Physics Research*, A267:351, 1988.

[45] K. Yasuoka *et al.* Response Maps of the CDF Central Electromagnetic Calorimeter with Electrons. *Nuclear Instruments and Methods in Physics Research*, A267:315, 1988.

[46] R. G. Wagner *et al.* Cosmic Ray Test of the CDF Central Calorimeter. *Nuclear Instruments and Methods in Physics Research*, A267:330, 1988.

[47] T. Devlin *et al.* Phototube Testing for CDF. *Nuclear Instruments and Methods in Physics Research*, A268:24, 1988.

[48] G. Ascoli *et al.* CDF Central Muon Detector. *Nuclear Instruments and Methods in Physics Research*, A268:33, 1988.

[49] K. Byrum *et al.* The CDF Forward Muon System. *Nuclear Instruments and Methods in Physics Research*, A268:46, 1988.

[50] G. Ascoli *et al.* A Leveling System for the CDF Central Muon Chambers. *Nuclear Instruments and Methods in Physics Research*, A268:41, 1988.

[51] G. Drake *et al.* CDF Front End Electronics: The RABBIT System. *Nuclear Instruments and Methods in Physics Research*, A269:68, 1988.

[52] E. Barsotti *et al.* Fastbus Data Acquisition for CDF. *Nuclear Instruments and Methods in Physics Research*, A269:82, 1988.

[53] D. Amidei *et al.* A Two-level Fastbus Based Trigger System for CDF. *Nuclear Instruments and Methods in Physics Research*, A269:51, 1988.

[54] G. Ascoli *et al.* CDF Central Muon Level-1 Trigger Electronics. *Nuclear Instruments and Methods in Physics Research*, A269:63, 1988.

[55] G. W. Foster *et al.* A Fast Hardware Track-finder for the CDF Central Tracking Chamber. *Nuclear Instruments and Methods in Physics Research*, A269:93, 1988.

[56] B. Flaugher *et al.* Integration of the ACP Multiprocessor Farm with the CDF Fastbus Data Acquisition System. In *IEEE Transactions on Nuclear Science*, page 865, 1987.

[57] J. T. Carroll *et al.* Level 3 System at CDF. *Nuclear Instruments and Methods in Physics Research*, A263:199, 1988.

[58] F. Abe *et al.* Measurement of W-boson Production in 1.8-TeV $p\bar{p}$ Collisions. *Physical Review Letters*, 62(9):1005, 1989.

[59] L. Nodulman. Scan of a Subset of 1 Inverse Picobarn of ZEN Missing Et Data. 1989. CDF note 846.

[60] Thomas J. Phillips. COSFLT: A Cosmic Ray Filter Using Charge Fraction. 1989. CDF note 1001.

[61] F. Abe *et al.* Measurement of the Ratio $\sigma(w \rightarrow e\nu)/\sigma(z \rightarrow ee)$ in $p\bar{p}$ Collisions at $\sqrt{s}$ = 1.8 TeV. *Physical Review Letters*, 64(2):152, 1990.

[62] F. A. Berends, W. T. Giele, H. Kuijf, R. Kleiss and W. J. Stirling. Multijet Production in W,Z Events at $p\bar{p}$ Colliders. *Physics Letters B*, 224(1,2):237, 1989.

[63] C. Newman-Holmes and J. Freeman. A Fast Calorimeter Simulation for SSC Detector Design. 1987. Fermilab preprint: Fermilab-Conf-87/231.

[64] Divid Brown, Marjorie Shapiro and Sheila Kannappan. QFL Version 2.0: Improvements and Checks. 1988. CDF Note 753.

[65] Brian L. Winer and Paul L. Tipton. Inclusive W Boson Production at Root s = 1.8 TeV: Status Report. September 1989. CDF note 1048.

[66] Howard Baer and Xerxes Tata. Component Formulae for Hadroproduction of Left- and Right-handed Squarks. *Physics Letters*, 160B(1,2,3):159, 1985.

[67] Xerxes Tata, Howard Bear and Jeffrey Woodside. Effect of Cascade Decays on the Fermilab Tevatron Gluino and Squark Mass Bounds. *Physical Review Letters*, 63(4):352, 1989.

[68] G. B. Gelmini, D. V. Nanopoulos, H. Baer, John Ellis and Xerxes Tata. Squark Decays into Gauginos at the $p\bar{p}$ Collider. *Physics Letters*, 161B(1,2,3):175, 1985.

[69] Kaoru Hagiwara, Howard Baer and Xerxes Tata. Gauginos as a Signal for Supersymmetry at $p\bar{p}$ Collider. *Physical Review D*, 35(5):1598, 1987.

[70] G. Zech. Upper Limits in Experiments with Background or Measurement Errors. *Nuclear Instruments and Methods in Physics Research*, A277:608, 1989.

Vita

Ping Hu

1962	Born November 14 in Beijing, China.
1980	Graduated from The Fifth High School, Beijing, China.
1980-85	Attended University of Science and Technology of China, Hefei, Anhui, China.
1985	B.S., University of Science and Technology of China.
1985-90	Graduate study at Rutgers, the State University of New Jersey, New Brunswick, New Jersey.
1985-89	Graduate Fellow, Rutgers, the State University of New Jersey.
1987-90	Publications (attached).
1989-90	Research Assistant, Department of Physics and Astronomy.
1990	Ph.D. in Physics, Rutgers, the State University of New Jersey.

PUBLISHED PAPERS

1. **Integration of the ACP Multiprocessor Farm with the CDF Fastbus Data Acquisition System**
by B. Flaugher, P. Auchincloss, A. Beretvas, T. Devlin, P. Hu, U. Joshi, T. Watts, J.T. Carroll, M. Larwill, S. Miyashita, Y. Morita, IEEE Transactions on Nuclear Science, **NS-34**, 865-869 (1987).

2. **The CDF Detector: An Overview**
by The CDF Collaboration, Nuclear Instruments and Methods, **A271**, 387-403 (1988).

3. **Transverse Momentum Distribution of Charged Particles Produced in $\bar{p}p$ Interactions at $\sqrt{s}$ = 630 and 1800 GeV** by The CDF Collaboration, Physical Review Letters **61**, 1819-1822 (1988).

4. **Measurement of the Inclusive Jet Cross Section in $\bar{p}p$ Collisions at $\sqrt{s}$ = 1.8 TeV** by The CDF Collaboration, Physical Review Letters **62**, 613-616 (1989).

5. **A Measurement of W Boson Production in 1.8 TeV $\bar{p}p$ Collisions** by The CDF Collaboration, Physical Review Letters **62**, 1005-1008 (1989).

6. **Limits on the Masses of Supersymmetric Particles from 1.8 TeV $p\bar{p}$ Collisions** by The CDF Collaboration, Physical Review Letters **62**, 1825-1828 (1989).

7. **Dijet Angular Distributions from $\bar{p}p$ Collisions at $\sqrt{s}$ = 1800 GeV** by The CDF Collaboration, Physical Review Letters **62**, 3020-3023 (1989).

8. **Measurement of the Mass and Width of the Z^0 Boson at the Fermilab Collider** by The CDF Collaboration, Physical Review Letters **63**, 720-723 (1989).

9. **Search for Heavy Stable Charged Particles in 1.8-TeV $p\bar{p}$ Collisions at the Fermilab Collider** by The CDF Collaboration, Physical Review Letters **63**, 1447-1450 (1989).

10. **K^0_s Production in $\bar{p}p$ Interactions at $\sqrt{s}$ = 630 and 1800 GeV** by The CDF Collaboration, Physical Review **D40**, 3791-3794 (1989).

11. **A Search for the Top Quark in the Reaction $\bar{p}p \rightarrow$ Electron + Jets at $\sqrt{s}$ = 1.8 TeV** by The CDF Collaboration, Physical Review Letters **64**, 142-146 (1990).

12. **A Search for New Heavy Quarks in Electron-Muon Events at the Fermilab Tevatron Collider** by The CDF Collaboration, Physical Review Letters **64**, 147-151 (1990).

13. **Measurement of the Ratio $\sigma(W \to e\nu)/\sigma(Z \to ee)$ in $\bar{p}p$ Collisions at $\sqrt{s}$ = 1.8 TeV** by The CDF Collaboration, Physical Review Letters **64**, 152-156 (1990).

14. **Two Jet Differential Cross Section in $\bar{p}p$ Collisions at $\sqrt{s}$ = 1.8 TeV** by The CDF Collaboration, Physical Review Letters **64**, 157-160 (1990).

15. **A Measurement of D^* Production in Jets from $\bar{p}p$ Collisions at $\sqrt{s}$ = 1.8 TeV** by The CDF Collaboration, Physical Review Letters **64**, 348-352 (1990).

16. **Search for a Light Higgs Boson at the Tevatron Proton-Antiproton Collider** by The CDF Collaboration, Physical Review **D41**, 1717-1721R (1990).

17. **The Two Jet Invariant Mass Distribution at $\sqrt{s}$ = 1.8 TeV** by The CDF Collaboration, Physical Review **D41**, 1722-1725R (1990).

18. **Pseudorapidity Distributions of Charged Particles Produced in $\bar{p}p$ Interactions at $\sqrt{s}$ = 630 and 1800 GeV** by The CDF Collaboration, Physical Review **D41**, 2330-2333R(1990).

CDF Collaboration - February, 1988

F.Abe[p], D.Amidei[c], G.Apollinari[k], G.Ascoli[g], M.Atac[d], P.Auchincloss[n], A.R.Baden[f], A. Barbaro-Galtieri[i], V.E.Barnes[l], E.Barsotti[d], F.Bedeschi[k], S.Behrends[l], S.Belforte[k], G.Bellettini[k], J.Bellinger[q], J.Bensinger[b], A.Beretvas[n], P.Berge[d], S.Bertolucci[e], S.Bhadra[g], M.Binkley[d], R.Blair[a], C.Blocker[b], J.Bofill[d], A.W.Booth[d], G.Brandenburg[f], A.Brenner[d], D.Brown[f], A.Byon[l], K.L.Byrum[q], M.Campbell[c], R.Carey[f],
W.Carithers[i], D.Carlsmith[q], J.T.Carroll[d], R.Cashmore[1], F.Cervelli[k], K.Chadwick[l], T.Chapin[m],
G.Chiarelli[k], W.Chinowsky[i], S.Cihangir[o], A.G.Clark[d], T.Collins[d], D.Connor[j], M. Contreras[b], J.Cooper[d], M.Cordelli[e], M.Curatolo[e], C.Day[d], R.DelFabbro[k], M.Dell'Orso[k],
L.DeMortier[b], T.Devlin[n], D.DiBitonto[o], R.Diebold[a], F.Dittus[d], A.DiVirgilio[k], R.Downing[g],
G. Drake[d], T.Droege[d], M.Eaton[f], J.E.Elias[d], R.Ely[i], S.Errede[g], B.Esposito[e], A.Feldman[f],
B.Flaugher[n], E.Focardi[k], G.W.Foster[d], M.Franklin[g], J.Freeman[d], H.Frisch[c], Y.Fukui[h], I.Gaines[d],
A.F.Garfinkel[l], P.Giannetti [k], N.Giokaris[m], P.Giromini[e], L.Gladney[j], M.Gold[i], K.Goulianos[m],
J.Grimson[d], C.Grosso-Pilcher[c], J.Grunhaus[7], C.Haber[i], S.R.Hahn[j], R.Handler[q], R.M.Harris[i],
J.Hauser[c], Y.Hayashide[p], T.Hessing[o], R.Hollebeek[j], L.Holloway[g], P.Hu[n], B.Hubbard[i], P.Hurst[g], J.Huth[d],
M.Incagli[k], M.Ito[p], J.Jaske[q], H.Jensen[d], R.P.Johnson[d], U.Joshi[n], R.W.Kadel[d], T.Kamon[o], S.Kanda[p],
D.A.Kardelis[g], I.Karliner[g], H.Kautzky[d], K.Kazlauskis[n], E.Kearns[f], R.Kephart[d], P.Kesten[b], H.Keutelian[g],
Y.Kikuchi[p], S.Kim[p], L.Kirsch[b], S.Kobayashi[3], K.Kondo[p], U.Kruse[g], S.E.Kuhlmann[l], A.T.Laasanen[l],
W.Li[a], T.Liss[c], N.Lockyer[j], F.Marchetto[o], R.Markeloff[q], L.A. Markosky[q], M.Masuzawa[p],
P.McIntyre[o], A.Menzione[k], T.Meyer[o], S.Mikamo[h], M.Miller[j], T.Mimashi[p], S.Miscetti[e], M.Mishina[h], S.Miyashita[p], H.Miyata[p], N.Mondal[q], S.Mori[p], Y.Morita[p], A.Mukherjee[d], A.Murakami[3], Y.Muraki[4], C.Nelson[d], C.Newman-Holmes[d], J.S.T.Ng[f], L.Nodulman[a], J.O'Meara[d],
G.Ott[q], T.Ozaki[p], S.Palanque[6], R.Paoletti[k], A.Para[d], J.Patrick[d], R.Perchonok[d], T.J.Phillips[f],
H.Piekarz[b], R.Plunkett[m], L.Pondrom[q], J.Proudfoot[a], G.Punzi[k], D.Quarrie[d], K.Ragan[j], G.Redlinger[c],
R.Rezmer[a], J.Rhoades[q], F.Rimondi[2], L.Ristori[k], T.Rohaly[j], A.Roodman[c], H.Sanders[c],
A.Sansoni[e], R.Sard[g], A.Savoy-Navarro[6], V.Scarpine[g], P.Schlabach[g], E.E.Schmidt[d], P.Schoessow[a],
M.H.Schub[l], R.Schwitters[f], A.Scribano[k], S.Segler[d], M.Sekiguchi[p], P.Sestini[k], M.Shapiro[f],
M.Sheaff[q], M.Shibata[p], M.Shochet[c], J.Siegrist[i], V.Simaitis[g], J.K.Simmons[l],

P.Sinervo[j],
M.Sivertz[5], J.Skarha[q], K.Sliwa[d], D.A.Smith[g], R.Snider[c], L.Spencer[b], R.St.Denis[f], A.Stefanini[k],
Y.Takaiwa[p], K.Takikawa[p], S.Tarem[b], D.Theriot[d], J.Ting[c], P.Tipton[i], A.Tollestrup[d], G.Tonelli[k],
W.Trischuk[f], Y.Tsay[c], K.Turner[d], F.Ukegawa[p], D.Underwood[a], C.vanIngen[d], R.VanBerg[j],
R.Vidal[d], R.G.Wagner[a], R.L.Wagner[d], J.Walsh[j], T.Watts[n], R.Webb[o], T.Westhusing[g], S.White[m], V.White[d], A.Wicklund[a], H.H.Williams[j], T.Winch[q], R.Yamada[d], T.Yamanouchi[d], A.Yamashita[p], K.Yasuoka[p], G.P.Yeh[d], J.Yoh[d], F.Zetti[k]

CDF Member Institutions

[a] Argonne National Laboratory- [b] Brandeis University- [c] University of Chicago
[d] Fermi National Accelerator Laboratory- [e] INFN, Frascati, Italy
[f] Harvard University- [g] University of Illinois- [h] KEK, Japan
[i] Lawrence Berkeley Laboratory-[j] University of Pennsylvania
[k] INFN, University and Scuola Normale Superiore of Pisa, Italy- [l] Purdue University
[m] Rockefeller University- [n] Rutgers University- [o] Texas A&M University
[p] University of Tsukuba, Japan- [q] University of Wisconsin

Visitors

[1] Oxford University, England- [2] INFN Bologna, Italy- [3] Saga University, Japan
[4] ICRR, Tokyo University, Japan- [5] Haverford College, Haverford, PA.
[6] CEN, Saclay, France- [7] University of Tel-Aviv, Israel